

Karoline Øverlie Edøy

# Separation-on-a-chip: coalescence and the influence of demulsifiers in w/o emulsions studied by advanced microfluidic methods

Master's thesis in Chemical Engineering

Supervisor: Gisle Øye, Jone Waage, Marcin Dudek

June 2020



Karoline Øverlie Edøy

# **Separation-on-a-chip: coalescence and the influence of demulsifiers in w/o emulsions studied by advanced microfluidic methods**

Master's thesis in Chemical Engineering  
Supervisor: Gisle Øye, Jone Waage, Marcin Dudek  
June 2020

Norwegian University of Science and Technology  
Faculty of Natural Sciences  
Department of Chemical Engineering







# Preface

This thesis is submitted at the Norwegian University of Science and Technology (NTNU), and is based on work completed over the spring semester at the Ugelstad Laboratory, Department of Chemical Engineering.

I received my bachelor's degree in Chemical Engineering from NTNU, and was accepted as a master student at the Ugelstad Laboratory in August 2019 under supervision of Gisle Øye and co-supervision Marcin Dudek. Aker BP has been an industrial partner with Jone Waage as an external supervisor.

# Acknowledgements

I would like to thank my supervisor professor Gisle Øye for accepting me as a master student in the Ugelstad group, and for your helpful guidance during the master's thesis.

I want to thank my external supervisor Jone Waage for showing interest in the project and for your valuable assistance.

I express my gratitude to my co-supervisor Marcin Dudek for your high competence in microfluidics. Thank you for never losing faith in this project. Your help and patience have truly been essential for my completion.

Thank you to the lab engineers for your help with administrative work and instrument training.

I am truly grateful for the assistance I received from Simon Våge at MI Swaco Schlumberger in Bergen. Thank you for inviting me to your laboratory.

I would like to thank my fellow master students Birgitte Vikse and Hanne Skudal Ullaland for support and encouragements throughout this year.

Last but not least, thank you to my family, friends and my dear Håkon.

# Sammendrag

Petroleumsindustrien produserer betydelig store mengder vann ved produksjon av olje, og dermed vil oljeemulsjoner være tilstede i reservoarene. Siden emulsjoner er termodynamisk ustabile, kreves det energitilførsel for å danne de. Da oljeproduksjonen inkluderer flere kilder for turbulente strømninger, gir dette opphav til dannelse av vann-i-olje emulsjoner. Da råoljen inneholder overflateaktive komponenter som kinetisk stabiliserer disse emulsjonene, forhindrer dette koagulering av de dispergerede vanndråpene i oljen. Det vil dermed være vanskelig å forhindre dannelse av slike emulsjoner. Den produserte vannfraksjonen har stor innvirkning både på kvaliteten på råoljen, og fører til høye energikostnader i oljeproduksjonen. Vannet vil også føre til problemer relatert til korrosjon i rørledninger og andre prosesseringsenheter. Ulike destabiliseringsmetoder implementeres for å oppnå faseparasjon mellom vann og olje. Kjemisk demulsifisering er en ofte benyttet metode som innebærer tilsetning av en overflateaktiv emulsjonsbryter for å øke destabilisering. Emulsjonsbryteren destabiliserer fasene ved å erstatte de stabiliserende overflateaktive oljekomponentene og øker muligheten for koagulering av de dispergerede vanndråpene i oljen. Den kjemiske demulsifiseringen gjennomføres ved konvensjonelle flasketester, men en ny metode som studerer dråpekoagulering i mikro-skala har nå blitt utviklet.

Dette prosjektet gikk ut på å utvikle mikrofluidiske metoder for å studere koagulering av vanndråper i en kontinuerlig oljefase. Eksperimentene ble komplementert og verifisert av konvensjonelle flasketester utført i fordypningsprosjektet under høstsemesteret. I tillegg til kvarts-mikrobalanse- og overflatespenningsmålinger, for å undersøke om den nyutviklede "lab-on-a-chip" teknologien potensielt kan benyttes kommersielt.

Den eksperimentelle delen inkluderte modifiseringer av den mikrofluidiske metoden for å tilrettelegge for optimale flow forhold for vann-i-olje systemer. Testene involverte regulering av temperatur, og dispergert- og kontinuerlig flowhastigheter for å vurdere koagulering ved å variere ulike parametre.

En sammenligning mellom den konvensjonelle flasketestmetoden og den mikrofluidiske metoden viser at sistnevnte gir flere fordeler ved studering av destabiliseringsfenomener, ulike kinetiske parametre og effektiviteten til ulike produksjonskjemikalier. Metoden inkluderer små prøvemengder og rask analysetid som gir store fordeler i petroleumsindustrien.

## Abstract

As the petroleum industry produces significantly large amounts of water compared to oil, crude oil emulsions are highly present in the reservoir fluids. As emulsions are thermodynamically unstable and do not form spontaneously, they require energy input. The oil processing includes a variety of mixing sources which enhance the creation of shear forces, hence promote crude oil emulsion formation. Due to the presence of indigenous compounds in the crude oil which kinetically stabilize the emulsions, the phenomena is difficult to prevent. The water fraction is highly unfavorable as it leads to high energy costs in the oil production, and problems related to corrosion in pipelines and other processing units. Different destabilization methods are implemented to obtain phase separation. Chemical demulsification is a commonly used method which involves addition of a surface-active chemical demulsifier to enhance destabilization. The components have the ability to replace the stabilizing natural surface-active agents in the crude oil, and improve destabilization. The chemical demulsification may be tested with the conventional bottle test. Or a recently developed technology which includes the study of droplet coalescence kinetics assessed in micro-scale.

This thesis aims to develop microfluidic methods to study droplet coalescence of water in a continuous crude oil phase. The experiments are complemented and verified by conventional bottle test measurements which were performed in the specialization project last autumn semester. In addition to quartz-crystal microbalance and interfacial tension measurements to investigate if the new "lab-on-a-chip" technology may potentially be used commercially.

The experimental part included modifications of the microfluidic method to facilitate optimum flow conditions for water-in-oil systems. The tests involved adjustments of temperature, and dispersed and continuous flow rates to assess the coalescence behaviour by varying different parameters.

A comparison between the conventional bottle test and the microfluidic method, shows that the latter method includes several benefits for studying destabilization phenomena, kinetic parameters and the efficiency of different production chemicals. The method includes small sample volumes, fast analysis time and automatic functionalities which serve advantages in the petroleum industry. If further improvements and developments were implemented, the method could become a potential substitute for the bottle test.

# Table of Contents

<b>1</b>	<b>Introduction</b>	<b>1</b>
<b>2</b>	<b>Background</b>	<b>2</b>
2.1	Crude oil . . . . .	2
2.1.1	Crude Oil Formation . . . . .	2
2.1.2	Crude Oil Production . . . . .	3
2.1.3	Crude Oil Composition . . . . .	6
2.2	Emulsions . . . . .	8
2.2.1	Emulsion Formation . . . . .	8
2.2.2	Emulsion Stability . . . . .	11
2.2.3	Emulsion Separation . . . . .	12
<b>3</b>	<b>Demulsification in Petroleum Industry</b>	<b>15</b>
3.1	Conventional Demulsification Methods . . . . .	15
3.2	Demulsifying Materials . . . . .	17
3.2.1	Oil-Water Interfacial Properties . . . . .	17
3.2.2	Demulsifier Characterization . . . . .	18
3.2.3	Hydrophilic-Lipophilic Balance . . . . .	19
3.2.4	Interaction Energies . . . . .	20
3.3	Influential Parameters . . . . .	21
3.3.1	Agitation . . . . .	21
3.3.2	Concentration of Demulsifier . . . . .	21
3.3.3	Droplet Size and Distribution . . . . .	22
3.3.4	Oil/Water Ratio . . . . .	22
3.3.5	Temperature . . . . .	23
3.3.6	Salinity . . . . .	23
3.4	Analytical Techniques for Studying Demulsification . . . . .	24
3.4.1	Bottle Test . . . . .	24
3.4.2	NMR Spectroscopic Techniques . . . . .	24
3.4.3	Near Infrared Spectroscopic Technique . . . . .	24
3.4.4	Microfluidic Methods . . . . .	25
<b>4</b>	<b>Methodology</b>	<b>26</b>
4.1	Microfluidic Measurements . . . . .	26
4.1.1	Chip Characterization . . . . .	28
4.2	Interfacial Tension Measurements . . . . .	30
4.3	Quartz Crystal Microbalance . . . . .	31

4.3.1	Quartz Crystal Microbalance with Dissipation . . . . .	32
<b>5</b>	<b>Experimental Methods</b>	<b>33</b>
5.1	Crude Oil Characterization . . . . .	33
5.2	Chemical Demulsifiers . . . . .	34
5.3	Sample Preparation . . . . .	35
5.4	Microfluidic Measurements . . . . .	36
5.4.1	Experimental setup . . . . .	36
5.4.2	Chip Design . . . . .	37
5.4.3	General Microfluidic Procedure . . . . .	39
5.4.4	Data Acquisition and Image Analysis . . . . .	39
5.4.5	Cleaning Procedure . . . . .	40
5.5	Interfacial Tension Measurements . . . . .	42
5.5.1	Experimental setup . . . . .	42
5.5.2	Sample Preparation . . . . .	42
5.5.3	Spinning Drop Procedure . . . . .	43
5.5.4	Cleaning Procedure . . . . .	44
5.6	Quartz Crystal Microbalance . . . . .	45
5.6.1	Experimental Setup . . . . .	45
5.6.2	Quartz Crystal Microbalance Procedure . . . . .	46
5.6.3	Cleaning Procedure . . . . .	46
<b>6</b>	<b>Results and Discussion</b>	<b>47</b>
6.1	Interfacial Tension Measurements . . . . .	47
6.2	Quartz Crystal Microbalance . . . . .	50
6.3	Microfluidic Measurements . . . . .	56
6.3.1	Method Development . . . . .	56
6.3.2	3D-Printed Chips . . . . .	59
6.3.3	Modification of Method . . . . .	62
6.3.4	Main Results . . . . .	69
6.4	Complementary Bottle Test Results . . . . .	74
<b>7</b>	<b>Conclusion</b>	<b>77</b>
	<b>Bibliography</b>	<b>79</b>
	<b>Appendix A Chip Design</b>	<b>88</b>
	<b>Appendix B Calculation</b>	<b>90</b>

## List of Figures

1	Upstream, midstream and downstream oil production [1]. . . . .	3
2	Upstream oil recovery. . . . .	4
3	Conventional SARA analysis. . . . .	6
4	Chemical structure of asphaltene and resin fractions [2]. . . . .	7
5	W/O and O/W crude oil emulsions. . . . .	8
6	Destabilization phenomena [3]. . . . .	12
7	Coalescence between two dispersed droplets [4]. . . . .	14
8	Scheme of chip design 2 used in the microfluidic experiments. . . . .	28
9	Reaction mechanism in hydrophobic coating between OTS and a substrate [5]. . . . .	29
10	Schematic illustration of the principle of the spinning drop video tensiometer [6]. . . . .	30
11	Schematic illustration of the working principle of QCM-D [7]. . . . .	32
12	Process overview. . . . .	33
13	Scheme of the microfluidic setup [8]. . . . .	36
14	Scheme of bottom plate for chip design 2. . . . .	38
15	Experimental setup of spinning drop video tensiometer. . . . .	42
16	Experimental setup of QCM-D. . . . .	45
17	IFT vs. time for demulsifier solutions in crude oil at 5 and 25 ppm. . . . .	47
18	Equilibrium IFT values for demulsifier solutions in crude oil at 5 and 25 ppm. . . . .	48
19	Frequency change for demulsifiers in crude oil. . . . .	50
20	Dissipation change for demulsifiers in crude oil. . . . .	51
21	Frequency and dissipation change for demulsifiers in xylene. . . . .	52
22	Adsorbed mass for xylene/demulsifier and crude oil/demulsifier. . . . .	54
23	Detected particles in flow channels. . . . .	56
24	Problems with hydrophobic coating and generation of initial droplet sizes. . . . .	58
25	Problems with hydrophobic coating and generation of initial droplet sizes. . . . .	59
26	3D-printed chip design 2. . . . .	61
27	Chip designs with different channel configurations. . . . .	62
28	Water flow behaviour from the continuous oil flow tests. . . . .	64
29	Coalescence frequency for dispersed flow rate tests at 3 and 4 $\mu\text{l}/\text{min}$ . . . . .	65
30	Coalescence frequency for a given temperature range. . . . .	67
31	Results from temperature tests performed at 8 and 10 $\mu\text{l}/\text{min}$ . . . . .	68

32	Droplet count for detection of coalescence for dispersed flow rates at 3 and 4 $\mu\text{l}/\text{min}$ . . . . .	69
33	Droplet count for detection of coalescence for dispersed flow rates at 8 and 10 $\mu\text{l}/\text{min}$ . . . . .	69
34	Droplets in size class 1 and 2. . . . .	70
35	Volume% of size class 1 and 2 droplets at dispersed flow at 8 $\mu\text{l}/\text{min}$ . . . . .	71
36	Volume% of size class 1 and 2 droplets at dispersed flow at 10 $\mu\text{l}/\text{min}$ . . . . .	72
37	Separated volume at 40% water cut. . . . .	74
38	Separated volume at 50% water cut. . . . .	74
39	Separated volume at 60% water cut. . . . .	75
40	Scheme of top standard plate. . . . .	88
41	Scheme of bottom plate for chip design 1. . . . .	88
42	Scheme of bottom plate for chip design 3. . . . .	89



## List of Tables

1	Physical properties of crude oil [9]. . . . .	33
2	Physical properties of demulsifiers [10], [11]. . . . .	34
3	Film layer thickness. . . . .	54

## List of Abbreviations

CMC	Critical Micelle Concentration
EOR	Enhanced Oil Recovery
GC	Gas Chromatography
HLB	Hydrophilic-Lipophilic Balance
HPLC	High-Performance Liquid Chromatography
IFT	Interfacial Tension
KF	Karl Fischer
LH	Layer Height
LW	Line Width
NCS	Norwegian Continental Shelf
NIR	Near InfraRed
NMR	Nuclear Magnetic Resonance
NTNU	Norwegian University of Science and Technology
OTS	OctadecylTrichloroSilane
O/W	Oil-in-Water
O/W/O	Oil-in-Water-in-Oil
PAH	Polycyclic Aromatic Hydrocarbon
PLA	Polyactic Acid
ppm	Parts Per Million
QCM	Quartz Crystal Microbalance
QCM-D	Quartz Crystal Microbalance - Dissipation
SARA	Saturates, Aromatics, Resins, Asphaltenes
SLB	Schlumberger
SDS	Sodium Dodecyl Sulfate
TD NMR	Low Resolution Time Domain Nuclear Magnetic Resonance
UMP	Universal Microfluidic Platform
UV	Ultraviolet

WAT	Wax Appearance Temperature
WC	Water Cut
W/O	Water-in-Oil
W/O/W	Water-in-Oil-in-Water

# 1 Introduction

The crude oil which is produced from the crude oil reservoirs contains high water fractions. The presence of the water has a significant impact on the quality of the crude oil including flow assurance problems due to the content of inorganic salts and dissolved  $\text{CO}_2$  and  $\text{H}_2\text{S}$  present in the water phase. These agents will accelerate the corrosion in pipelines through an electrochemical reaction which leads to material degradation [12]. The main problem of the presence of water is separation problems of crude oil and the water. Crude oil emulsions which are produced in the petroleum industry are highly unfavorable, and the presence of surface-active components such as asphaltenes and resins found in the crude oil have a stabilizing effect on the crude oil emulsions. The components make the separation of the two phases rather difficult, and several techniques are implemented to break the crude oil emulsions. Chemical demulsification includes addition of surface-active components which improve destabilization by enhancing coalescence of water droplets in the continuous oil phase [3].

The efficiency of demulsifiers is commonly assessed through stability analysis such as the bottle test. A recent developed technology which study the chemical demulsifier performance in droplet coalescence kinetics assess the destabilization phenomena in micro-scale. The technology is termed "lab-on-a-chip", and integrates lab-scale functionalities into small chips with microchannels [13]. Additional methods were performed to allow better mechanistic understanding of the systems. Quartz crystal microbalance measurements were done to assess the hydrophilic affinities, and interfacial tension measurements were done to obtain information about the ability of adsorption.

## 2 Background

### 2.1 Crude oil

Crude oil is a mixture of geological deposits of hydrocarbons and other organic materials. Even though the composition varies depending on the geological migration conditions and crude oil sources, the mixtures contains elemental species. The elemental proportions vary over fairly narrow limits, but the composition range can be classified into carbon (83 - 87%), hydrogen (10 - 14%), nitrogen (0.1 - 2%), oxygen (0.05 - 1.5 %), sulfur (0.05 - 6.0%) and organometallic complexes such as nickel and vanadium (< 1000 ppm) [14],[15], [16]. The assessment of the crude oil characterization is quite demanding due to the considerable wide range of crude oil compositions which vary for different reservoirs and oil fields [15].

#### 2.1.1 Crude Oil Formation

Crude oil has its origin from aquatic plants, animals and other organic materials deposited as sediments on the seabed. The decomposition process requires high temperature and pressure to undergo breakdown and transformation [17].

The Norwegian Continental Shelf (NCS) consists of a thick layer of black clay that lies under the seabed. The black clay are deposits of organic residual and acts as a source rock for crude oil formation. Through bacterial decomposition of dead accumulated microscopic phytoplankton in the sediment, the formation of liquid and gaseous hydrocarbons is present in the source rock of black clay [17].

The crude oil and gas oppose the weight of the rock deposits, as the hydrocarbons are lighter compared to the water. It creates migration upward inside the porous network with permeable rocks. The flowing fluid may be hindered and entrapped during migration if the sedimentary rocks include cap rocks which consist of impermeable material inside a reservoir. The accumulation of crude oil creates several layers, where the bottom layer includes water, the middle layer consists of crude oil and gas, and the top layer contains gas. As the reservoir rocks include changes in both porosity and permeability, they will differ in position, depth and width. A suitable combination of source rock, reservoir rock and cap rock gives the possibility of discovery of recoverable oil and gas deposits [17]. A series of reservoir rocks is commonly called an oil field, and the production of crude oil depends on the characteristics of the series of reservoir rocks [18].

## 2.1.2 Crude Oil Production

The oil industry is classified into upstream, midstream and downstream production of oil. The term upstream production includes subsea exploration and drilling followed by upgrading of the crude oil by separation and injection of production chemicals. The midstream segment is referred to as storage and transportation of crude oil from fields to downstream production which involves refining and processing to high-valuable products [1]. Figure 1 shows a schematic of the upstream, midstream and downstream processing steps.

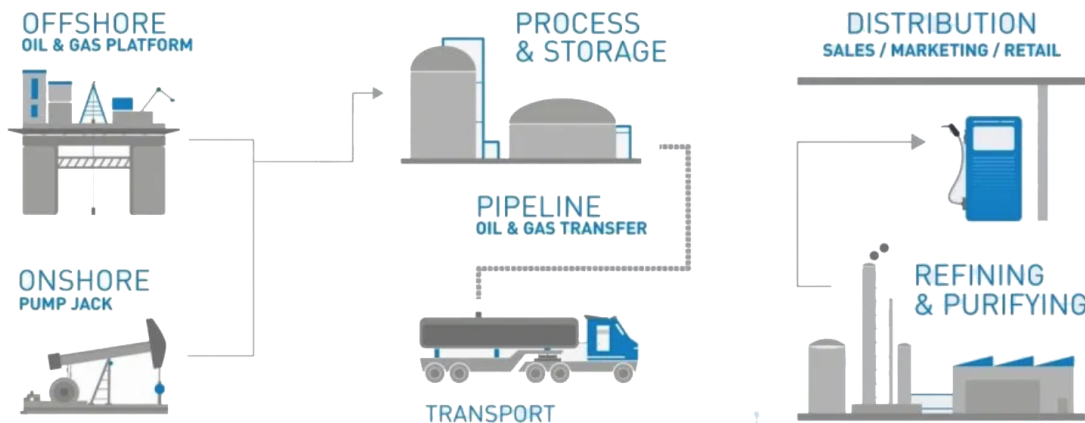


Figure 1: Upstream, midstream and downstream oil production [1].

### Upstream Production

The upstream production involves exploration of crude oil and natural gas fields, as well as production and recovery [1]. The upstream production mainly focuses on drilling and operation of wells for further recovery of crude oil and gas. After a successful seismological acquisition, a production well is drilled. There are several types of drilling techniques. Multilateral wells are suited for subsea production and offshore installations. A multilateral well comprises more than one wellbore which is connected to a main bore [19]. If the operator discovers more wells within range, it is possible to install branches through laterals from the main well bore to have the ability to maximize the production of the reserves [20]. The upstream oil recovery can be divided into three methods: primary, secondary and enhanced oil recovery shown in Figure 2 [18].

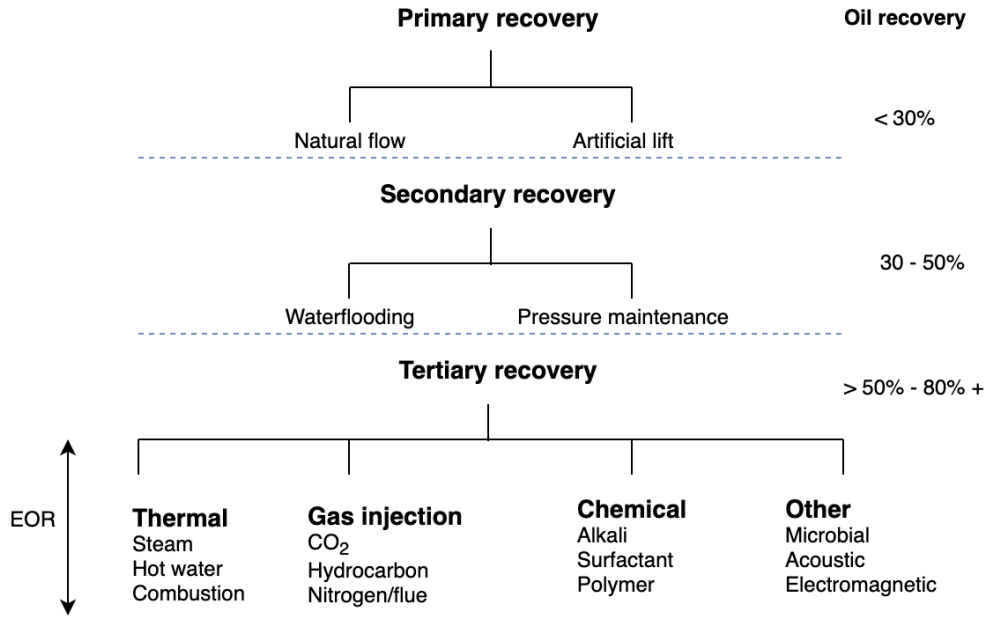


Figure 2: Upstream oil recovery.

- Primary oil recovery includes extraction of crude oil by natural mechanisms through pressurization in the reservoir rock. The mechanical methods depend on the availability of energy in the reservoir. Reservoir rocks with a high gas content experience high pressure. They require a lower energy input compared to reservoir rocks with low pressure. Overall, the primary oil recovery results in a relatively low recovery of the crude oil as the driving forces may be quite inefficient in reservoirs with lack of energy [21]. To obtain a complete recovery of crude oil, primary recovery has to be complemented with secondary and tertiary recovery methods [18], [22].

- The secondary oil recovery methods involve addition of mechanical devices to promote an increase of pressure in the reservoirs [23]. As the rock reservoirs age, they experience a pressure drop due to drainage of fluids. Complementary wells are drilled to maintain and increase the pressure in the rock reservoir to create a sufficient flow of crude oil to the production wells. The increase of internal pressure is caused by injection of immiscible gas or water [24]. The injection methods are referred to as waterflooding and gas injection. Waterflooding includes external energy contributions into the reservoir formation by injection of water for displacement of residual oil. Gas injection takes place in the gas cap. The flooding techniques create potential problems due to variable permeability in the reservoir formation which limit the oil recovery [25].

- During oil production, the flow through an oil reservoir is mainly dominated by the relative permeability. A multiphase flow of fluid in a porous media is characterized by the separate critical points of the two fluids such as the ratio of viscosity, the distribution of grain size, interfacial tension and contact angle by wettability [26]. The enhanced oil recovery (EOR) methods use sophisticated techniques by considering the rheological properties of the oil and reservoir to improve fluid flow and oil displacement [27], [28].

### **Midstream Production**

The midstream sector in the oil industry mainly focuses on storage and transport of upstream produced crude oil and gas. The midstream operations connect the upstream and downstream production, and generally start where the produced hydrocarbons enter a transportation system either underwater by pipelines, or above water by vehicles, tankers or barges. The transportation of crude oil through pipelines requires no excess of water, and a maximum water content at 0.5 to 2.0 %. The midstream sector ends where the transported hydrocarbons enter downstream refinery storage tanks [29],[1].

### **Downstream Production**

The downstream distribution sector primarily involves product preparation and usage through refining and purifying [1]. Separation, conversion, treating and blending are some processes implemented in a complex refinery plant [30]. The goals for the refining are to operate the processes in a safe, economically feasible and environmentally acceptable manner [29]. The refining involves a complex manufacturing of gasoline, kerosene, jet fuel, diesel oil, waxes, asphalt and other petrochemical products [31].



### 2.1.3 Crude Oil Composition

Crude oils are complex mixtures with compositions depending on the geological location of oil fields [32]. The assessment of composition is important for structure property, optimization of performance evaluation and refining processes, including prediction of flow assurance problems in the upstream crude oil production [33].

Fractionation is a useful technique to assess crude oil compositions, and for development of standard analytical procedures for research. SARA fractionation which is based on sequential separation, classifies the indigenous components which are referred to as saturates, aromatics, resins and asphaltenes, respectively. The component groups are distinct due to aromaticity, polarity and solubility [33]. SARA fractionation includes precipitation of asphaltenes by using n-alkanes such as n-pentane and n-heptane as solvents. The lighter fractions; the saturates, aromatics and resins get eluted through chromatographic columns with various polarity filled with solvents. The technique is called a high-performance liquid chromatography (HPLC). The saturates are separated from the other components by flushing n-alkanes through the column. Toluene separates the adsorbed aromatic fraction in the column, and the resins are eluted with solvents such as methanol and chloroform which tend to have high polar characteristics [34]. Figure 3 shows the conventional SARA analysis.

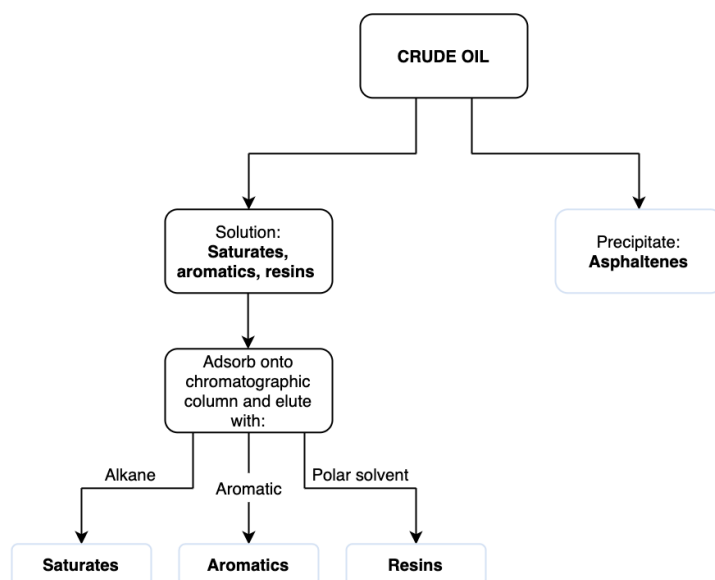


Figure 3: Conventional SARA analysis.

The **saturate** fraction contains mostly aliphatic compounds which are straight-chained hydrocarbons. The fraction of saturates presents the lightest and less polar constituent in crude oil.

The **aromatic** fraction involves hydrocarbons with aromatic groups and aliphatic side chains. All crude oils contain some amounts of aromatic constituents [33].

The **resin** fraction contains heteroatoms such as nitrogen, oxygen and sulfur. As the resins have a high H/C ratio and an intermediate polarity, a desorption of resins from asphaltene aggregates leads to precipitation. The resins have important bulk properties which attribute to the stability of the crude oil [33].

The **asphaltene** fraction is highly complex and polar. The complex mixtures vary depending on their origin and recovery. Due to its complexity it causes problems in association with oil processing. The fraction tends to form aggregates due to stabilization. The self-aggregation is induced by stabilizing constituents such as resins. The stable aggregates exhibit interfacial activity which stabilizes water-in-crude oil emulsions [33],[35].

The resin and asphaltene fractions differ due to their tendency of solubility, polarity and chemical structure. Resins are soluble in heavy n-alkanes such as n-heptane and n-pentane, but insoluble in lighter hydrocarbons such as liquid propane. Asphaltenes are insoluble in n-alkanes, but soluble in toluene. The polarizability plays an important role, as it increases from the light to the complex hydrocarbons. Their chemical structures are different, as asphaltenes are complex mixtures which vary based on their origin and recovery [36],[35]. Their structure mainly include condensed polycyclic aromatic hydrocarbons (PAHs) with alkyl chains. On the other hand, resins consist of smaller molecules composed of fused aromatic rings, branched paraffins and polar compounds. Their chemical structures are shown in Figure 4.

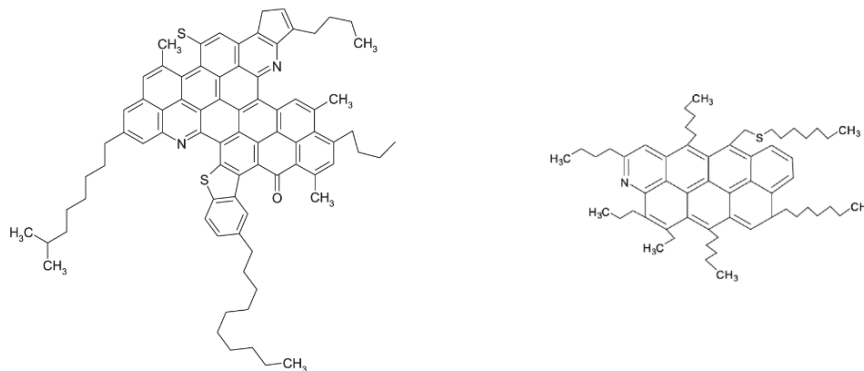


Figure 4: Chemical structure of asphaltene and resin fractions [2].

## 2.2 Emulsions

Emulsions are dispersed systems which consist of two or more immiscible liquids [37]. Crude oil emulsions are often undesirable in the oil industry as it causes issues related to separation of the two phases. The separation problems affect the crude oil quality [38].

Crude oil emulsions produced in oil fields can be categorized into water-in-oil (W/O), oil-in-water (O/W) and complex and multiple emulsions such as oil-in-water-in-oil (O/W/O) and water-in-oil-in-water (W/O/W) [39]. The nature of dispersed and continuous phase classifies the type of emulsion. W/O emulsions include a continuous oil phase and a dispersed water phase. While O/W emulsions consist of a water continuous phase with dispersed oil droplets. The more complex emulsions have small dispersed droplets in larger dispersed droplets in a continuous phase [40]. Figure 5 shows schematics of W/O and O/W crude oil emulsions.

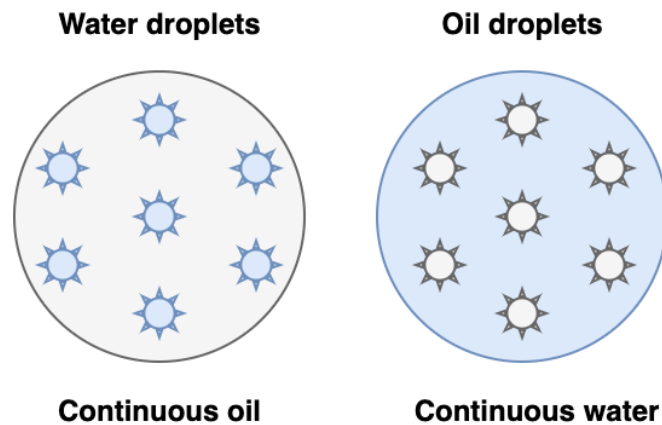


Figure 5: W/O and O/W crude oil emulsions.

### 2.2.1 Emulsion Formation

Formation of W/O emulsions will be present in the upstream and midstream production in the oil industry due to the high amounts of produced water in the produced fluids. The emulsion formations create challenges due to flow characteristics of multiphase flows [32], [41]. As the production involves emulsifying agents and shear forces, the droplet size distribution and interfacial properties impair the possible collision forces between the immiscible liquids, hence promote formation of emulsions [40]. Generally, three criterias are emphasized for formation of crude oil emulsions [37].

- Contact between two immiscible liquids, such as oil and water.
- Presence of a surface active component which acts as an emulsifying agent.
- Energy input to create droplets in a continuous liquid phase.

### **Emulsifying Agents**

When surfactants, natural surface-active agents or finely divided solids are present in an emulsion, they will affect the interfacial properties between the two phases [37].

**Surfactants** are usually organic compounds composed of a hydrophilic group which interact with the water phase, and a hydrophobic group which has a tendency to interact with the crude oil phase. As they have surface-active properties, they adsorb on surfaces and interfaces to alter the surface properties by reducing the surface tension or interfacial tension (IFT) [42]. The surfactants may be classified according to their head group; anionic, cationic, nonionic and zwitterionic [43].

Anionic surfactants are commonly used in chemical EOR processes due to their low affinity to reservoir rocks of sandstone. Cationic surfactants are not used in sandstone reservoirs as they have a tendency to strongly adsorb in sandstone rocks. Generally, they are used in carbonate rocks to change the wettability of the reservoir from oil-wet to water-wet. As mixtures with anionic and nonionic surfactants prove to be highly effective, they are often used on systems with high salinity. Nonionic surfactants are mostly used as cosurfactants to enhance system phase behaviour. This class of surfactants is more tolerant of high salinity compared to anionic surfactants [44].

The content of **natural surface-active agents** in crude oil is highly related to the formation of emulsions. The asphaltenes have the ability to reduce the interfacial tension of a system by creating a film between two immiscible phases. The adsorption is generally irreversible and much slower compared to surfactant adsorption. The interfacial film has sufficient mechanical strength which induces the stabilization of the emulsion. The asphaltene-stabilized emulsions reaches a maximum stability before precipitation of asphaltenes. Above the limit for precipitation, the asphaltene fractions precipitate and less molecules are available to cover the interface and improve stability. Other crude oil components such as acidic compounds, resins, porphyrins and wax crystals have a tendency to associate with the asphaltene components, and affect the stability of the crude oil emulsion. In general, the resin fraction prevents crude oil emulsion stability, but an addition of such components may cause resolubilization of partly precipitated asphaltenes. The sta-

bility will not be improved if the additional amount of resins are too high [39]. Wax which consists of long-chain saturated hydrocarbons, and acidic fractions such as the naphthenic acids and the fatty acids which naturally occur in the crude oil, do affect the emulsion stability [3].

**The finely divided solids** in crude oil originate from microbial activity in the reservoir, and corrosion products, drilling muds and mineral scales from oil production. Precipitation in the oil production contributes to the amount of fine solids that may lead to formation and stabilization of emulsions. The fine solids have the ability to mechanically stabilize the emulsions by accumulating at the interface between the crude oil and water phase. The fine solid materials should be smaller than the emulsion droplets to obtain complete wetting of the molecules. At higher particle concentrations, the possibility for formation of multilayers are present, which guarantee a highly stable emulsion [39]. Factors such as size distribution and interaction between particles contribute to increase the effectiveness of the finely divided stabilizing solids [45].

### **Shear Forces**

As emulsions are thermodynamically unstable and do not form spontaneously, they require energy input. There are several emulsification methods such as simple manual shaking, mixing with electronic or high pressure devices and liquid injection through porous membranes. The oil processing includes a variety of mixing sources which enhance the creation of shear forces. The production implements the forces through flow lines, tubings and production headers. Pumps, valves and chokes are process units that create disturbance in multiphase flows. The shear forces induce the tendency of stabilization of the formed crude oil emulsions during processing [37]. Emulsification occurs when the droplet size is small enough that collision forces which act on the molecules in the medium prevent settling of the dispersed droplets, hence destabilization of the emulsion [37], [46].

### 2.2.2 Emulsion Stability

Stable emulsions are strongly undesired phenomena in the petroleum industry, but interfacial active fractions will be present in the systems. From a thermodynamic point of view, an emulsion is considered to be an unstable system due to the natural inclination for dispersion due to reduction of interfacial area. The crude oil-produced emulsions may be classified due to their kinetic stability and level of divergence [47].

There are several parameters which either decrease or increase the emulsion stability, steric stability and electrostatic stability. The dynamic elasticity and viscosity of the system affected by deformation of surfaces and circulation of droplets. The emulsion stability and viscosity are affected by droplet size and distribution. By increasing the speed and mixing interval, one obtains a reduction in diameter size due to interactions of particles in two different phases. Adjustment of temperature does also have a large impact on the emulsion stability. High system temperatures lead to an increase of the discrepancy between the dispersed and continuous phase, and rise the tendency for droplet collisions as the interfacial film gets weakened. The presence of solid particles increases the rigid interfacial film, hence prevents destabilization. However, the emulsion properties change slowly in the unstable systems which leads to separation through different destabilization phenomena [41].

### 2.2.3 Emulsion Separation

Destabilization of an emulsion by addition of a surfactant depends on the appearance of deformation of the interfacial film. The process is based on a two-step mechanism which is given below.

- Adsorption of surfactant at the interface between two liquid phases, due to high affinity to the surface.
- Emulsion breakage by disruption of the surface network which contains stabilizing molecules. The destabilization takes place through demulsification mechanisms.

The interaction between two interacting emulsion droplets occurs by intermolecular forces such as Van der Waals, steric, structural and electrostatic. The interaction leads to either rebound, creaming, sedimentation or flocculation before coalescence takes place [40]. The destabilization mechanisms are shown in Figure 6.

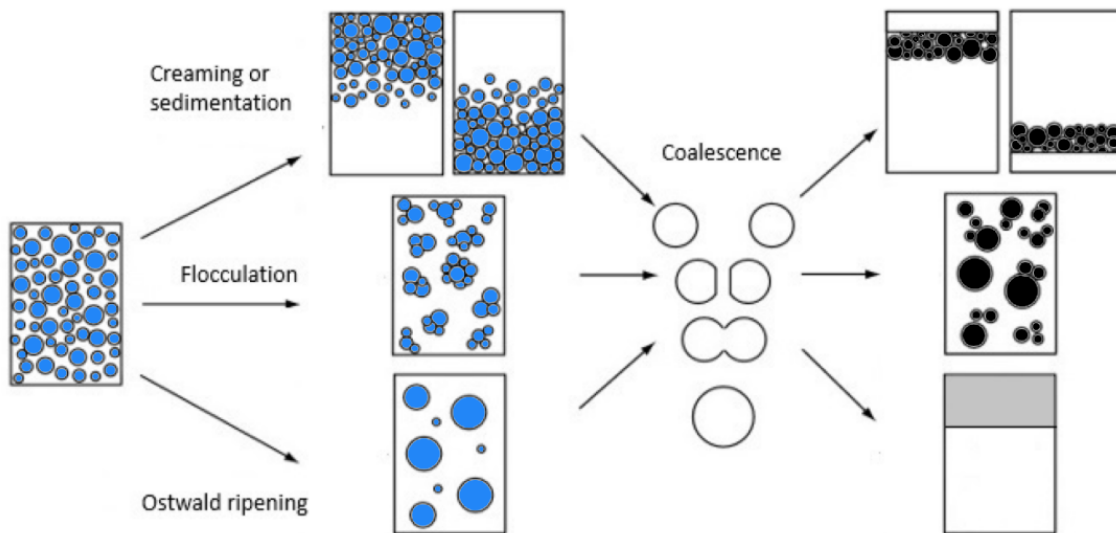


Figure 6: Destabilization phenomena [3].

## Sedimentation and Creaming

Sedimentation and creaming are demulsification mechanisms which occur due to difference in specific gravity. A reduction in interfacial energy between two phases occurs through migration of settling water droplets in a W/O emulsion. The gravitational and bouyancy forces are affected by a frictional force which counteracts the gravitational force which result in a balance between two active forces [48]. The balance is presented by Stokes law shown in Equation 1.

$$V_{Stokes} = \frac{(\rho_d - \rho_c) \cdot g d^2}{18\mu_c} \quad (1)$$

$V_{Stokes}$  presents the sedimentation velocity,  $\rho_d$  is the density of the dispersed phase,  $\rho_c$  is the density of continuous phase,  $d$  is the particle diameter,  $g$  is the gravitational constant and  $\mu_c$  is the viscosity of the continuous phase [49].

The creaming and sedimentation mechanisms are depending on the density difference. The oil droplets in a O/W emulsion float to the top of the emulsion by creaming, if the density difference is negative. While a positive difference causes sedimentation of water droplets in W/O emulsions [50].

## Flocculation

Flocculation is a destabilization process where the dispersed droplets aggregate in an energetically stable state. The phenomena is present when the repulsion between the aggregated droplets is weaker compared to the Van der Waals attraction. The droplet-droplet interaction may be facilitated by Brownian motion, which is random and thermal movement of the colloidal particles [51], [52].

As a high amount of water will cause an increase in droplet size, it will also induce the probability of flocculation. A low dispersed phase fraction gives a stable emulsion due to low flocculation frequency, according to the phase volume theory about emulsion stability. Addition of thermal energy promotes flocculation by increasing the internal entropy of the system which is emphasized by the influential parameters for a chemical demulsifier [53] [54].



## Coalescence

The coalescence behaviour between two droplets can be divided into three main parts. The continuous liquid between two dispersed droplets drains out by external flow, Brownian motion or buoyancy. The hydrodynamic step creates a surface concentration gradient of surfactant molecules. The gradient leads to a surface tension gradient which creates stress at the interface between the droplets. The stress caused by the surface tension gradient is called the Marangoni effect. The interface between the two droplets will eventually interact when the film has reached a significantly low thickness [48]. The two interfaces will undergo interaction through surface forces. The interfacial film reaches an equilibrium thickness when the Van der Waals forces and repulsive forces are present. The final step in the destabilization mechanism is a thermally activated process which involves nucleation of a pore in the thin film that bridges the droplets. The droplets will eventually fusion together when the critical thickness of the film layer is achieved, and the surface film gets considerable small [40], [55]. A visualization of coalescence between two droplets is shown in Figure 7.

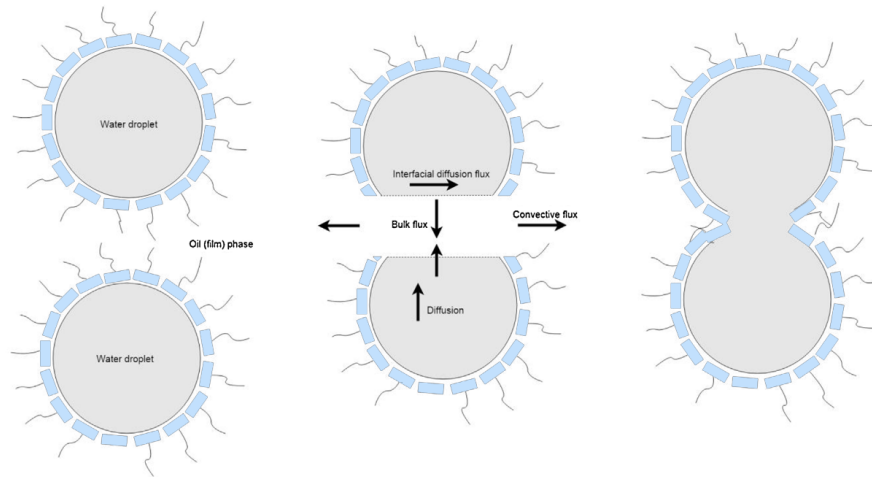


Figure 7: Coalescence between two dispersed droplets [4].

### 3 Demulsification in Petroleum Industry

Efficient demulsification processes are well acknowledged in the oil industry, due to the difficulties associated with emulsion formation. If a demulsification process does not run, several problems concerning the oil processing will arise. The crude oil emulsions with high viscosity may cause pressure growth, corrosion and catalyst poisoning. If the crude oil contains high amounts of water, it will lead to a high content of basic sediments in the refining processes which causes high cost of pumping and vessel heating [3].

There are several demulsification methods, and the effectiveness is assessed by observing the ability in reducing the emulsion stability until complete separation. The influential factors of the droplet size distribution and stability must be understood to obtain an optimal separation of a specific crude oil emulsion. The conventional demulsification methods are gravity separation, electrocoalescence, thermal treatment and chemical demulsification [3], [56].

#### 3.1 Conventional Demulsification Methods

**Gravity Separation** is a method based on the difference in densities between two liquids in a crude oil emulsion. The liquid with highest specific gravity creates a settling rate which separates the coalesced water droplets from the crude oil phase. Gravity separation requires a favorable flow pattern and a sufficient residence time of the system [57].

**Electrocoalescence** is a conventional method used for treating crude oil emulsions. The technique involves activation of electric fields to speed up droplet attraction and coalescence in a crude oil emulsion for phase separation [24]. Electrical and mechanical forces which act on the droplets, in addition to bulk properties of the medium, induce drag forces which promote phase separation. When droplet coalescence takes place, it increases the settling rate of water which enhances demulsification [58].

**Thermal Treatment** methods include increasing the system temperature to decrease the oil viscosity. The water settling rate increases, hence promotes phase separation. High thermal energy of the droplet is a parameter which affects the coalescence frequency by increasing it significantly [57].

**Chemical Demulsification** is a common method to promote phase separation. Chemical demulsifiers are added to break or counteract the stabilizing layers around the droplets by adsorption to the interface. Appropriate chemical demulsifying materials are designed for specific crude oil emulsions to obtain a cost-effective and rapid separation. The rheological and dynamic properties of surfactant adsorption which affects the elasticity, surface viscosity and diffusivity are major factors which need to be considered when studying the demulsification under dynamic conditions. The procedure to get an effective demulsification is listed in the following steps below [59].

- A sufficient amount of a chemical demulsifier must be added.
- Homogenization of demulsifying material and emulsion by addition of energy.
- The phase separation may be accelerated by addition of thermal energy.
- Adequate residence time for settling of water droplets.

## 3.2 Demulsifying Materials

Surface-active agents such as demulsifiers are surfactants which promote separation. Demulsification involves adsorption of a surfactant to an interface between two immiscible fluids, reduction of interfacial tension and hydrophobicity to enhance wetting properties. The adsorption causes a decrease in viscosity of the interfacial film due to a replacement of the stabilizing molecules with surfactant molecules which promote phase separation [48]. The main objective for a demulsifier is to prevent the emulsification mechanism and facilitate droplet coalescence kinetics. The selection of an optimal demulsifier is crucial due to the large number of crude oil components [3].

### 3.2.1 Oil-Water Interfacial Properties

The interfacial tension can be defined as the Gibbs energy needed to increase the unit interfacial area between two immiscible liquids at constant pressure and temperature. It is the force of attraction between the molecules which is located at the interface of two liquids. The interfacial tension is expressed in Equation 2 [14].

$$\gamma = \left(\frac{\partial G}{\partial A}\right)_{n,T} \quad (2)$$

Where  $\gamma$  is the interfacial tension,  $G$  is the Gibbs free energy,  $A$  is the area of the interface,  $n$  is the constant composition and  $T$  is the temperature.

As the interface is considered to be dynamic, it consists of a highly viscous monolayer. The monolayer involves interfacial stress which acts on the layer and causes interfacial shear viscosity. The shear viscosity is expressed in Equation 3 [14].

$$\sigma_s = \eta_s \dot{\gamma} \quad (3)$$

..

Where  $\sigma_s$  is the interfacial stress,  $\eta_s$  is the interfacial shear viscosity and  $\dot{\gamma}$  is the shear rate.

The interfacial elasticity is another important factor when studying rheological behaviours of systems. When dilating the interface between the two droplets, the area decreases and the interfacial tension increases. The interfacial dilational (Gibbs) elasticity is given in Equation 4 [14].

$$\epsilon = \frac{d\gamma}{d\ln A} \quad (4)$$

Where  $\epsilon$  is the interfacial dilational (Gibbs) elasticity,  $d\gamma$  is the change in interfacial tension during expansion, and  $dA$  is an interfacial tension gradient.

A chemical demulsifier has the ability to decrease the interfacial elasticity when it is added to a crude oil emulsion due to deformation of a liquid interface. The elasticity is changed due to the replacement of the stabilizing emulsifying agents at the interfacial layer. As a result of the replacement, the strength, life time and thickness of the interfacial film will be reduced [60], [61].

The deformation of the film enhances interfacial dilatation by increasing the viscous dissipation in the gap between the two interacting droplets. The flattening is facilitated by high droplet sizes, low interfacial tension, high droplet-droplet attraction and the counteraction of droplet-droplet repulsion. The film will eventually break when the film thickness reaches a critical value [62].

### 3.2.2 Demulsifier Characterization

Chemical demulsifiers are developed specifically for individual emulsion systems. Surfactants are often used in optimization of separation processes. The demulsifying agents are chemicals which consist of an amphiphilic structure. They have a water-soluble head group and an oil-soluble carbon tail. Due to their affinity towards both the water and oil phase, they are able to break the layer formation around the droplets and adsorb faster than the crude oil components [48].

### 3.2.3 Hydrophilic-Lipophilic Balance

The hydrophilic-lipophilic balance (HLB) is a numerical term used to classify the chemical emulsion breakers. The range includes values from 0 to 20 which represent the balance of size and strength of the two amphiphilic parts of a surfactant molecule [63]. The number indicates the tendency to solubilize in oil or water, and thus their tendency to create W/O or O/W emulsions. Surfactants with a low HLB value correspond to a hydrophobic molecule which tend to be soluble in oil. These chemicals will form W/O emulsions. A chemical surfactant with 20 as a HLB value does completely consist of hydrophilic components and form O/W emulsions. The concept of HLB can be summarized by Bancrofts rule which says that surfactants that are solubilized in the oil phase prefer formation of W/O emulsions, and opposite for the water solubilized surfactants [64]. The surfactant properties based on HLB values are listed below [48].

0 - 3	<b>Antifoaming agent</b>
4 - 6	<b>W/O emulsifier</b>
7 - 9	<b>Wetting agent</b>
8 - 18	<b>O/W emulsifier</b>
13 - 15	<b>Detergent</b>
10 - 18	<b>Solubilizer of hydrotrope</b>

The correlations between the demulsifying power and the chemical structure of a demulsifier are complicated due to different compositions of the crude oil and water phase [65]. The selection of a demulsifier for an oil requires a lot of screening work, and there are some general guidelines. For a surfactant to act as an emulsion breaker, it has to show strong affinity to the interfacial film between the water and crude oil phase. The attraction can be detected by studying the migration to the phase to reach the droplet interface where it counteracts the emulsifying agent [66].

The demulsifying materials are like emulsifying agents, categorized considering their chemical structure and the nature of the charge of the hydrophilic head group. This study will focus on the nonionic surfactants. The nonionic surfactants consist of a head group which carry no charge. The hydrophilic part is commonly based on poly(ethylene oxide) (EO). Due to a high number of hydrophilic moieties present, there is a lot of commercial nonionic surfacants available. Some of the most known commercial demulsifier formulations include Pluronic surfactants which consist of a tri-block copolymer structure. Their wide application range is due to their high tolerance for high salinity brine and low toxicity [67].

### 3.2.4 Interaction Energies

The separation efficiency is affected by substantial factors such as steric effects. As the nonionic surfactants include properties of isomerism, it influences the steric behaviour of the system. By addition of a nonionic surfactant with sequential PEO (polyethylene oxide) blocks to a W/O emulsion, it will create affinity to both the crude oil phase and the water phase. The hydrophilic group adsorbs to the water droplets, while the hydrophobic group attaches to the crude oil phase. As a result, a generation of an interfacial film with steric repulsion is formed. The steric repulsion is a result from unfavorable mixing of the PEO chains. A reduction in configurational entropy of the carbon chains may also be a cause for the formation of the steric repulsion [68] [69].

The steric repulsions are essential in the emulsion breaking, as they tend to counteract the Van der Waals attractions between the emulsion droplets. The Van der Waals forces take place between either atoms or molecules, and due to their strength, they can be classified into dipole-dipole (Keesom), dipole-induced (Debye) or dispersion interactions (London). All the dipoles have different orientations which tend to cancel out. London dispersions arise from charge fluctuations by continuous rotation of electrons around a nucleus in the atom, and is considered to be the strongest dipole force [70].

### **3.3 Influential Parameters**

The characterization of stability and demulsification performance depends on several parameters. The efficiency of a chemical demulsifier depends on agitation, concentration of demulsifier, oil and water content, temperature and salinity. Rheological characteristics such as droplet size and distribution are parameters which also play an important role for characterization of chemical demulsification [48].

#### **3.3.1 Agitation**

As emulsification requires energy by homogenizing, the agitation speed has an impact on the separation efficiency. A high input of energy creates a decrease of the size of the distributed water droplets in W/O emulsions. As the droplets get smaller, a more stable emulsion is created [48], [3].

#### **3.3.2 Concentration of Demulsifier**

If the crude oil emulsions are very stable, they require more to be destabilized. Chemical demulsification is an efficient method to counteract the stability. By increasing the concentration of demulsifier, it is possible to destabilize very stable emulsions. The dosage of demulsifier may be challenging due to the difficult identification of the optimum concentration. An overdosing may cause restabilization, while addition of a too small amount of chemical demulsifier may lead to no significant phase separation [71].

The dosage of chemical demulsifier does also depend on molecular weight and properties of adsorption such as the degree of hydrophilicity and hydrophobicity. The concentration of demulsifier and the salinity in the crude oil emulsion are related, as the salinity range in which a surfactant is interfacially most active, is a function of the molecular weight. The optimum salinity for production of a low interfacial tension gets reduced, as the molecular weight of the surfactant increases [72], [48].



### 3.3.3 Droplet Size and Distribution

Droplet size distribution is an important characteristic of emulsions as it determines the potential demulsification processes of a system. The size and distribution of droplets in crude oil emulsions affect the viscosity of the overall emulsion. Emulsions which consist of small droplet sizes have a high viscosity and are relatively stable [73]

The size distribution of dispersed droplets is an important factor when determining the dosage of demulsifier. Two emulsions with the same dispersed phase fraction, but with different distributions of droplet sizes, have different demands for the addition of a chemical demulsifier. Emulsions which contain small droplet sizes, but several droplets number-wise, requires a higher surface area to be covered, compared to emulsions with larger droplets and a lower total surface area [74], [73].

### 3.3.4 Oil/Water Ratio

Oil and water contents are important parameters when considering the efficiency of demulsification. The destabilization process gets accelerated when increasing the water content in a crude oil emulsion which contains an emulsion breaker. The principle emphasizes that emulsions with low amounts of water will be more stable compared to emulsions with a high water fraction. The rate of destabilization processes is promoted as the amount of dispersed droplets stays at a sufficiently high level. The number of dispersed droplets plays an important role for the potential change in entropy. High efficiency includes a high number of dispersed droplets, hence high probability for efficient collisions. The optimum crude oil and water contents for destabilization of a W/O emulsion are favored by a high water fraction and a separation of O/W emulsion is favored by a high crude oil fraction [48].

### 3.3.5 Temperature

The thermal energy affects the demulsification process in a great extent. As the crude oil consists of a wide variety of stabilizing components which coprecipitate with the heavy asphaltene fractions, application of thermal energy upon heat may lead to a reduction in viscosity of the crude oil phase. The reduction causes higher probability for collisions of water droplets in W/O emulsions and a weaker interfacial film due to the decreasing elasticity. The effect of temperature can vary from one system to another one [74]. Long chain saturated hydrocarbons called waxes are present below appearance temperature, and have the ability to interact with the oil/water interface. Hence, the precipitates favor emulsion stability and shows a significant resistance to droplet coalescence. Application of thermal energy prevents wax precipitation by avoiding the system to reach wax appearance temperature (WAT) [75]. The temperature and salinity of the system may be related. An increase in temperature causes a decrease in water and oil solubilization at optimum salinity.

A characteristic behaviour for nonionic surfactants with PO chains is their ability to exhibit reverse solubility due to breakage of the hydrogen-oxygen bonds at the hydrophilic group, when the surfactant molecular activity increases. The bond breakage leads to separation of surfactant molecules and the solution gets cloudy. Phase separation occurs when the cloud point is achieved.

### 3.3.6 Salinity

The salinity conditions are essential for the destabilization mechanisms. The phase behavior of emulsions is strongly affected by the salinity of the brine used in the water phase. The salinity affects the polymer viscosity, hence determines the potential emulsions a surfactant may form. As sodium chloride (NaCl) is the main salt in saline water, it is most common to use the mass of NaCl to decide the salinity of a specific system which contains saline water.

High salinity brine decreases the solubility of anionic surfactants. The surfactants exhibit sufficient water phase solubility at low salinity flooding, hence contribute to stabilize W/O emulsions. The solubilization increases with increasing hydrophobic length of the surfactants. Surfactants with weak PO chains have been characterized to lower the optimum salinity by having calcium tolerance. The addition of EO groups, or combined PO and EO groups show similar behaviour [15], [76].

## **3.4 Analytical Techniques for Studying Demulsification**

### **3.4.1 Bottle Test**

Bottle test is a conventional and easy technique for studying demulsification and efficiency of chemical surface-active substances. The method is based on the principle for gravity separation, and the objective is to study the settling rate of water phase from crude oil phase in presence of a chemical demulsifier. The testing is used to assess the amount of demulsifier needed to obtain a complete demulsification. Parameters such as oil/water ratio, temperature, and concentration of chemical demulsifier do have significant impacts on the breaking. During performance, it is important that the sample represents the actual studied emulsion. Therefore, the method is commonly performed offshore to ensure a fresh sample. By addition of agitation, one obtains a relative stable emulsion which is further monitored through phase separation as a function of time [77].

### **3.4.2 NMR Spectroscopic Techniques**

The technique includes application of a magnetic field to a system with an orthogonal radio frequency pulse. By studying these parameters, one can investigate the magnetization of nuclei of protons which exhibit a constant magnetic moment [78]. The spectroscopic method is required to characterize emulsions by droplet size distribution and dispersed phase ratio, among other things. Low Resolution Time Domain NMR (TD NMR) is a common technique used with the conventional bottle test method [79], [80].

### **3.4.3 Near Infrared Spectroscopic Technique**

The technique includes utilization of qualitative and quantitative analysis by Near Infrared (NIR), to monitor destabilization mechanisms of emulsions [78]. By studying the vibrational frequencies which are correlated to the stabilizing tendencies improved by natural surface-active agents and aggregation, one provides insight in demulsification mechanisms. The NIR spectral region includes 700 nm to 2500 nm, and depends on physical parameters such as particle dispersion. The technique can be applied for determination of particle size. The technique serves advantages such as simple and multiple analysis procedures, and analysis of both chemical and physical properties [81].

### 3.4.4 Microfluidic Methods

Recent research activities developed in micro-scale focus on surfactant and chemical demulsifier performance in droplet coalescence kinetics. The research of microfluidics had a considerable growth the last two decades. The technology is termed "lab-on-a-chip" as it integrates laboratory functions in a single microchannel chip. The chip includes a desired channel configuration which allows in-situ monitoring through oil droplet coalescence kinetics in crude oil emulsions. The chip design makes it possible to study the kinetics as a function of several emulsion properties such as viscosity and density. Also rheological properties such as film drainage efficiency, flux, size of droplets and volume fraction of dispersed phase are related to the overall kinetics of the system, and may be studied in microfluidic lab-on-a-chip technologies [78].

The development of microfluidic lab-on-a-chip techniques enables analysis with short experiment time and rapid adjustment of experimental conditions, among other things. The handling of small volumes provides the method health and safety benefits compared to traditional techniques which generally involve higher sample volumes. Another advantage related to the use of microfluidic methods, is the small size of the experimental setup which make on-site analysis possible [73].

## 4 Methodology

### 4.1 Microfluidic Measurements

Parameters concerning the kinetics are useful to study for assessing the separation of a crude oil emulsion. The kinetic parameters are especially important to address, but conventional separation methods may not be suited for those stability analysis. The bottle test does not emulate the external flow field which acts on the droplets. Gravity-based settling methods do also have difficulties with separation of crude oil emulsions which contain trace amounts of dispersed phase, as those systems consist of much larger gravitational force fields compared to the residence time in the separator.

Hence, a fast and easy experimental method to study crude oil emulsions is useful for optimization of process designs, further research of rheological properties and to assess separation efficiency and stability of emulsions in conventional separators used in the oil industry.

Microfluidic experiments are based on multiphase flow with microdroplets. The manipulation of the droplets refers to controlling small volume liquids with two immiscible fluids. The system includes one continuous and one dispersed phase. The microdroplets will undergo merging through collisions and drainage [82], [55].

Considering the fundamental differences between large-scale analysis and microfluidics, the physical properties related to multiphase flow are the most significant. The multiphase flow is characterized by separation of phases with interfaces in the flow field, which create nonlinear effects with complicated behaviour. The Reynolds number ( $Re$ ) is a dimensionless value used to predict flow behaviour in different flow systems. Low Reynolds numbers ( $Re < 2300$ ) predict laminar flow patterns, and high Reynolds numbers ( $Re > 4000$ ) are flow systems dominated by turbulence. The Reynolds number for a flow in a microfluidic chip can be calculated by Equation 5.

$$Re = \frac{\rho v l}{\eta} \quad (5)$$

Where  $Re$  is the Reynolds number,  $\rho$  is the density and  $\eta$  is the viscosity of the continuous phase,  $v$  is the velocity and  $l$  is the width of the coalescence chamber.

As the Reynolds number does not take into account the dispersed phase, the dimensionless Weber number is commonly used to predict flow behaviour of multi-phase systems which involve an interface between two different fluids. The Weber number can be calculated from Equation 6.

$$We = \frac{\rho v^2 l}{\sigma} \quad (6)$$

Where  $We$  is the Weber number,  $\rho$  is the density of the continuous phase,  $v$  is the velocity,  $l$  is the width of the coalescence chamber and  $\sigma$  is the interfacial tension.

In large scale applications will fluids mix convectively causing eddies and turbulence. As the microchannel walls in microfluidic experiment are quite limited, the multi-phase flow with microdroplets involves high mass and heat transfer, efficient and short diffusion distances and high monodispersity. The multiphase flow involves laminar behaviour by parallel flows. The only mixing which occurs is diffusion of molecules across the interface between the two phases [83], [8].

Considering the detection of drop coalescence, the development of high-speed imaging technologies implemented in the microfluidic methods has made it possible to monitor the phenomena. The possibility to create calibrated droplets through high flow rates in a two-dimensional network of channels provides conductance of statistical analyses of droplet coalescence which takes place in the channels. Hydrodynamical forcing in microfluidics is used to assess the stability of an emulsion which undergoes high flow rates.

When using high-speed imaging, one can measure the droplet size distribution at the end of a coalescence chamber [13]. The coalescence frequency in a microchannel is calculated from Equation 7 [8].

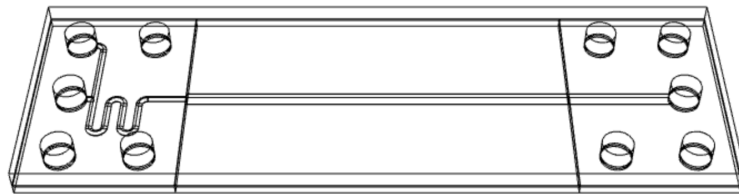
$$f = \frac{N_{in} - 1}{N_f T_{res}} \quad (7)$$

Where  $N_{in}$  is the number of initially created droplets,  $N_f$  is the actual number of droplets for each size class and  $t_{res}$  is the residence time of droplets in the chip channel.

### 4.1.1 Chip Characterization

One of the unique features of the microfluidic experiments is the several chip designs. By replacing a chip with another one with a different design, one can perform different lab-on-a-chip analyses. The chips used in microfluidic experiments for determination of coalescence frequency are commonly divided up in three parts. The inlet contains a T-junction which provides droplet generation at a cross-flow, and a meandering channel for droplet aging. The continuous and dispersed phases are mixed together from two inlet channels. The middle part includes a wider chamber. As the main channel is wider compared to the inlet meandered channel, it is possible for the droplets to undergo collisions, hence coalesce. The outlet part contains an extension of the main channel where the dispersed and coalesced droplets are lead to the outlet tubing [13], [8]. Chip design 2 was used in the main microfluidic experiments, and the designed 3D model is shown in Figure 8. The 3D modeling is explained in section 5.4.2.

Figure 8: Scheme of chip design 2 used in the microfluidic experiments.



### Hydrophobic Coating

As the glass chips consist of hydrophilic surfaces, water in crude oil systems face difficulties related to drop generation in chip experiments. The dispersed water phase would interact with the glass walls, hence resist generation of required water droplets. Therefore, hydrophobic coating is essential for such systems. The coating procedure involves chemisorption of organosilane molecules which consist of a long hydrocarbon chain and a silane head group. The silanization is substrate activation by wet chemical processing, in which the hydrophilic surfaces are immersed in solutions with silane molecules. The head groups adsorb to the hydrophilic surfaces, and form reactive silanol groups [84].

Octadecyltrichlorosilane (OTS) is a common chemical used in hydrophobic coating. It consists of a long hydrocarbon chain and a trichlorosilane head group which binds to the silicates in the glass wall. The coating mechanism includes dissolving the component in a solvent, hydrolyzing of Si-Cl bonds to Si-OH (silanol) groups by the trichlorosilane polar head groups [85]. Attraction to the oxidized hydrophilic surface causes formation of Si-O-Si (siloxane) links. As the siloxane groups condense with other groups, they produce covalent siloxane bonds which result in a strong hydrophobic surface on the precursor molecule [86]. A schematic of the reaction mechanism is shown in Figure 9.

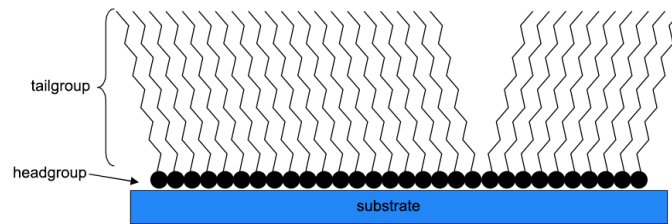


Figure 9: Reaction mechanism in hydrophobic coating between OTS and a substrate [5].



## 4.2 Interfacial Tension Measurements

The dynamic interfacial tension measurements are commonly implemented in experimental testing by using a spinning drop tensiometer. The procedure involves analysis of video imaging of a dispersed droplet in a continuous liquid placed in a rotating capillary. When the capillary spins, the resulting centrifugal forces increase and center the drop and deforms it to a cylindrical shape due to the density difference between the liquids [87], [88]. The centrifugal forces counteract the interfacial tension which results in elongation of the droplet [89], [90]. The resulting interfacial tension is a function of the drop shape, the rotation speed of the capillary and the densities of the two liquids [91]. The principle is shown in Figure 10.

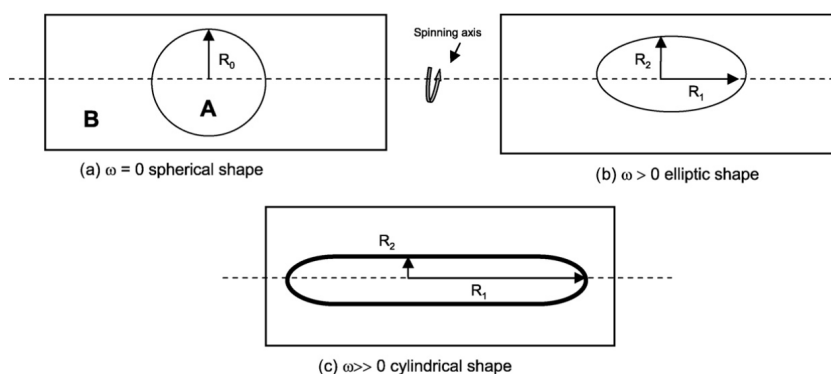


Figure 10: Schematic illustration of the principle of the spinning drop video tensiometer [6].

The interfacial tension can be calculated from the Young-Laplace equation which considers the curvature, surface energy and pressure difference between the two phases. The Young-Laplace equation is given in Equation 8 [6].

$$\sigma \left( \frac{1}{R_1} + \frac{1}{R_2} \right) = \frac{2\sigma}{R_0} + \Delta\rho\omega^2\lambda^2 \quad (8)$$

Where  $\sigma$  is the interfacial tension,  $(\Delta\rho\omega^2\lambda^2)$  is the centrifugal force on a volume element,  $R_0$  is the sphere radius, and  $R_1$  and  $R_2$  is the curvature radii. The equation is divided up into two terms, where the term on the right side represents the spherical conditions, and the left side contributes for the droplet deformation and hydrostatic pressure differences. The size of the interface changes during the experiment, and the instrument has the ability to specify the surface age over a long time range. In addition to find the dynamic interfacial tension of a system, the rotation speed and the drop deformation can be used to measure the interfacial elasticity and viscosity.

### 4.3 Quartz Crystal Microbalance

Quartz Crystal Microbalance (QCM) is a method based on monitoring mass balance due to changes in mass per unit area of a piezoelectric material such as quartz with a measurement surface of gold. By application of metal electrodes top coated with a high surface area of porous material, it has a tendency to oscillate at a defined frequency [92]. The frequency may change due to addition or removal of mass on the electrode surface. The relative change in frequency may signify molecular interactions or reactions which take place on the electrodes. Possible interactions are corrosion, oxidation or film growth. Film growth does occur either by formation of soft or rigid layers. Adsorption through vacuum or gas phase creates rigid film layers which is completely related to oscillation of the electrodes on the surface. Therefore, mass adsorption of rigid films are linearly connected to the change in frequency of oscillation [93], [7]. The relation is defined through Sauerbrey equation shown in Equation 9.

$$\Delta m = -C \cdot \Delta f / n \quad (9)$$

Where  $\Delta m$  is the mass of adsorbed layer,  $C$  is a constant related to quartz properties such as density and shear modulus,  $\Delta f$  is the resonance frequency change and  $n$  is an odd overtone number [94]. When the mass change is calculated, it is possible to determine the film layer thickness by taking into account the adsorbed volume and the surface area by using Equation 10 and 11.

$$V_{ads.layer} = \frac{\Delta m}{\rho} \quad (10)$$

$$h = \frac{V_{ads.layer}}{A_{surface}} \quad (11)$$

Where  $h$  is the layer thickness,  $\rho$  is the density of adsorbed layer,  $\Delta m$  is the mass change,  $V_{ads.layer}$  is the volume of the adsorbed layer and  $A_{surface}$  is the area of surface. The adsorption shows a rather different behaviour in liquid media, as it will get affected by molecular adsorption from associated liquid molecules. It results in viscoelastic films with high energy losses of the oscillation [7].

### 4.3.1 Quartz Crystal Microbalance with Dissipation

By monitoring the change in dissipation in addition to the change in frequency for samples with liquid environments, additional structural information can be obtained. The structural information is based on conformational changes in the film layer. The dissipation factor is based on dissipated energy per oscillation divided by the total stored energy of the system given in Equation 12. Hence, the film layer behaviour during oscillation will be related to the change in dissipation [7].

$$D = \frac{E_{dissipated}}{2\pi \cdot E_{stored}} \quad (12)$$

Where  $D$  is the dissipation factor,  $E_{dissipated}$  is the dissipated energy and  $E_{stored}$  is the stored energy in the oscillating system.

The quartz crystal microbalance with dissipation (QCM-D) provides information about the viscoelastic properties of the adsorbed mass layer through viscosity, elasticity and density. Viscoelastic adsorbed films on the quartz crystal deform and increase the dissipation. While rigid layers will not undergo deformation during oscillation, hence decrease the dissipation [7]. Figure 11 shows an overview of the principle of QCM-D measurements.

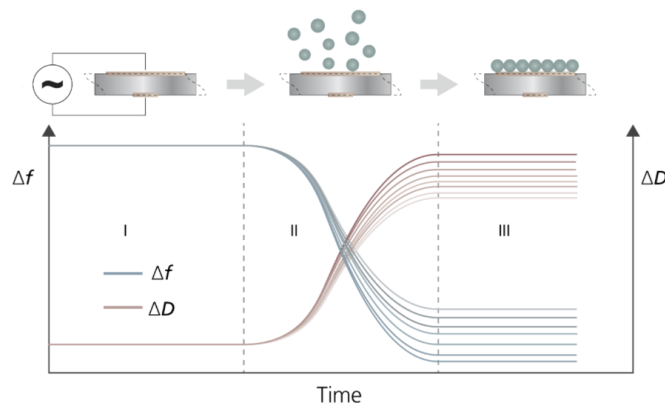


Figure 11: Schematic illustration of the working principle of QCM-D [7].

# 5 Experimental Methods

## 5.1 Crude Oil Characterization

The experimental methods were performed by using crude oil from one of Aker BP's assets at the Norwegian Continental Shelf (NCS). The crude oil sample was taken from a sample point located downstream for injection points of production chemicals. Hence, it was not possible to ensure a true representation of the drilled crude oil from the reservoir without any additives of chemical demulsifiers. Figure 12 shows a process overview with injection points of production chemicals, separation unit and sample point denoted with S.

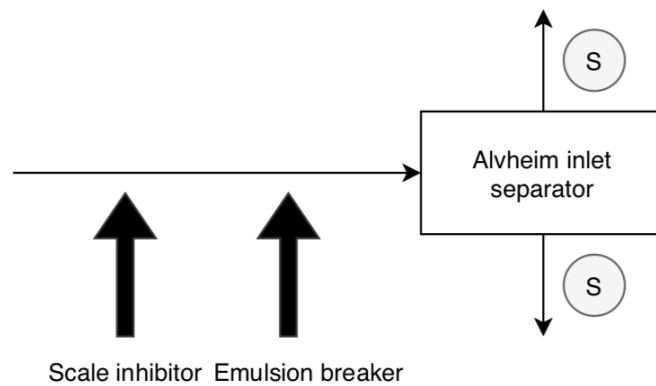


Figure 12: Process overview.

The physical properties and composition of the crude oil are summarized in Table 1.

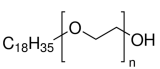
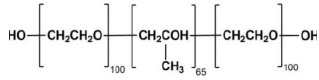
Table 1: Physical properties of crude oil [9].

Density (15°C)	Viscosity [mPa · s] (20°C)	Pour point [°C]	Water in oil [ppm]
0.846 g/cm <sup>3</sup>	12.4	<-5	1742.87

## 5.2 Chemical Demulsifiers

The chemical demulsifiers used in the study, are model and commercial chemicals. One of the demulsifiers was received from the chemical vendor Schlumberger, while the two other ones were available at Ugelstad Laboratory. Table 2 shows an overview of chemical structures, molecular weights, HLB values, densities and chemical structures for the three demulsifiers.

Table 2: Physical properties of demulsifiers [10], [11].

	Brij-93	EB-8075	Pluronic PE8100
Chemical structure	Polyethylene glycol ether	Received from SLB	Block copolymer
Molecular weight [g/mol]	357	-	2300
HLB	4	-	2
Density [g/cm <sup>3</sup> ]	0.912	0.978	1.030
Chemical Structure		-	

Brij-93 is a low-molecular surfactant with polyethylene glycol oleyl ether compounds. The chemical has a molecular weight at 357 g/mol and a HLB value at 4 [10].

EB-8075 is a commercial surfactant with unknown physical properties.

Pluronic PE8100 is a nonionic surfactant with a low-foaming characteristic provided by BASF. It is built up by polyoxyethylene polyoxypropylene polyoxyethylene (PEO PPO PEO), where the polypropylene glycol group is centered and flanked by two polyethylene groups. The chemical has a molecular weight at 2300 g/mol, and is considered to be a high-molecular demulsifier. The molecule has a HLB value at 2, and is provided to be one of the best wetting agents in the Pluronic series of chemical demulsifiers [11].

### 5.3 Sample Preparation

The **brine solution** was prepared by dissolving sodium chloride (NaCl) with deionized water to obtain a 3.5 wt% salt solution with a density at approximately 1.02 g/cm<sup>3</sup>.

The **demulsifier solutions** were prepared from stock solutions of 10 000 ppm dissolved in xylene. The demulsifier was transferred to a 50 ml Schott bottle, and xylene was added. The stock solution was diluted to 0.5 ppm, 2.5 ppm, 5 ppm and 25 ppm by transferring specific volumes of stock solution to 200 ml Schott bottles, and add with crude oil.

The **coating solution** contained 0.2 V% OTS in toluene, prepared by solution of 100  $\mu$ l octadecyltrichlorosilane (OTS) in 50 ml toluene. The coating procedure involved injection of coating solution with a plastic syringe to the chip which was placed in a chip holder with fittings and tubings. The coating solution remained in the chip for approximately 15 minutes before the solution was emptied and dried by injection of air from a new plastic syringe. The coating process resulted in lining of hydrocarbon chains to the glass walls, which promoted a hydrophobic surface fitted for water droplet generation in a continuous crude oil phase flow.

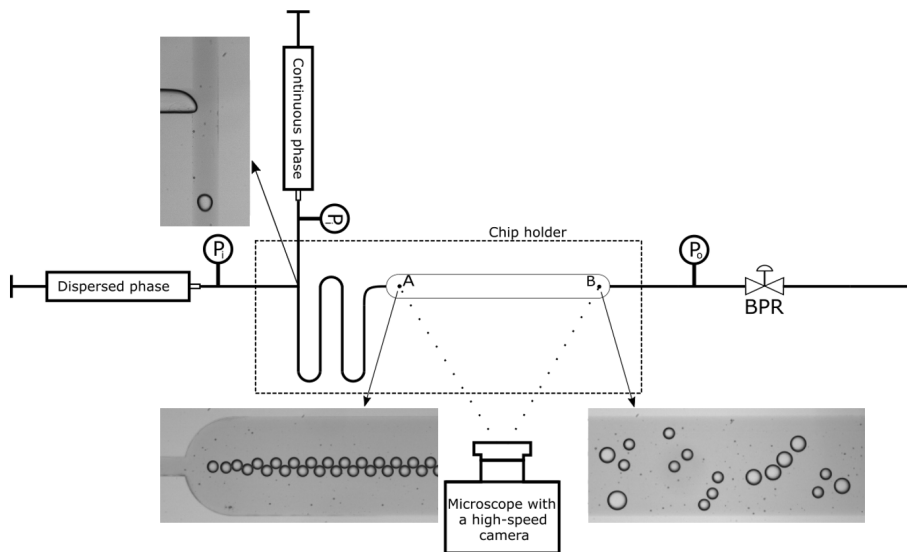
## 5.4 Microfluidic Measurements

### 5.4.1 Experimental setup

The microfluidic setup included components which posed the main required Universal Microfluidic Platform. It involved an inverted microscope (Nikon Ti-U), a high-speed camera (Photron AX100/Fastcam Mini), a flow setup, a computer-controlled software and microfluidic chips with several structure designs placed in chip holders (Micronit Microtechnologies). The microfluidic chip holders were connected to the flow setup by PEEK tubings and FFKM ferrules. The water and crude oil phases with chemical demulsifiers were injected by syringe pumps (neMESYS module V3).

Due to low heights of the channels in the chip, the high-speed imaging made it possible to visualize the occurring phenomena in the chip, by capturing 1000 - 500 000 frames per second [13], [8]. Figure 13 shows a scheme of the microfluidic setup for studying coalescence. The visualization includes the inlets for continuous and dispersed phase for chip design 2.

Figure 13: Scheme of the microfluidic setup [8].



### 5.4.2 Chip Design

The chip size is set by specific dimensions determined by the chip holder used in the microfluidic experiments. The microfluidic chips used in the experiment, were custom-made of glass (Micronit Microtechnologies). The inlet channels of water phase and crude oil phase had a width of 100  $\mu\text{m}$ , which became mixed in a T-junction where the generation of droplets took place. The droplets would further pass a meandering channel for droplet aging before entering a wider coalescence chamber with a width of 500  $\mu\text{m}$  and length of 33 mm, where the droplets could possibly undergo coalescence. All channels had a uniform depth at 45  $\mu\text{m}$ .

#### 3D-printed Chips

As the overall analysis time of the microfluidic tests mainly involves glass chip preparation and cleaning, 3D-printed chips in thermoplastic materials were designed and printed. The printing was performed to obtain information about the transparency of the chips, and see if the thermoplastic chips could potentially be applied in the microfluidic experiments.

Different chip designs were modified and assembled in the commercial software for 3D CAD modeling in Fusion 360 for 3D printing. Due to problems with transparency, the dimensions were modified to obtain wider transparent channels which could be detected in the microscope.

The modeling included three different chip designs with a standard top plate with a total of 10 tubing holes with a diameter at 2 mm. Two holes were used for the inlet water and oil tubings, and one hole for the outlet waste tubing. The bottom plates differed from each other as they included different dimensions of the main flow channels and meandering channels at the inlet part. The three chip designs had a constant length at 45 mm long, 15 mm width and a total height at 1.8 mm.

The top plate were modelled by creating a new sketch with given length and width. The plate was extruded to 1.1 mm, and the standard holes were drawn and extruded through the top plate. A schematic of the top standard plate is shown in Appendix A.





### 5.4.3 General Microfluidic Procedure

The microfluidic experiments were conducted with brine solution and original crude oil sample without chemical additive, and crude oil with chemical demulsifier concentrations at 0.5, 2.5, 5 and 25 ppm. The tests were performed at different flow rates of continuous phase (40 - 80  $\mu\text{l}/\text{min}$ ) and dispersed phase (2 - 10  $\mu\text{l}/\text{min}$ ) at room temperature to 60°C by using different glass chip designs.

The initial step for the microfluidic experiments, was to coat the glass chips with OTS solution in toluene (0.2 vol%). The coating was performed in a chip holder by injection of solution through tubings. After approximately 15 minutes was the solution emptied and dried with air before the glass chip was ready for testing.

After mounting the glass syringes and connecting the crude oil phase and water phase to the flow setup by tubings, a filling procedure was started. It filled and emptied the syringes several times to ensure pure phases and no air bubbles in the system. The glass chip was placed in the chip holder which was located in the microscope. The tubings were removed from the oil and water waste holders, and placed in the chip holder and connected to the glass chip with ferrules. After the syringes were filled and the glass chip was ready for testing, the manual adjustment of flow rates of dispersed and continuous phases started. By studying the coalescence chamber of the chip by microscope and monitoring the system pressure, one could detect the water droplets from the T-junction and at the inlet and outlet of the coalescence chamber. When the dispersed droplets got a stable flow behaviour, series of images were recorded at different locations of the coalescence chamber. All sequences were further processed in the ImageJ software.

### 5.4.4 Data Acquisition and Image Analysis

The ImageJ software was used for image analysis of recordings taken during experiment. The images were edited by adjusting the contrast and brightness to obtain black and white recordings of droplet flow. Hence, it became possible to count droplets in a window with adjustable width. The analysis of systems with flow rates of dispersed phase at 3 and 4  $\mu\text{l}/\text{min}$ , included image analysis of a series of 7058 recordings with a frame rate at 2000 frames/s from both inlet and outlet for approximately 3 seconds. The series of inlet images were used to determine the size and number of initial droplets, while the series of outlet images were used to determine the coalescence frequency. The droplet count at both inlet and outlet was limited to droplets with circularity at 0.7 - 1 and size area at 200  $\mu\text{m}^2$ - infinity, to

avoid detection of non-spherical droplets and unknown non-relevant particles in the system. The data from inlet and outlet was copied to an Excel-sheet in addition to the width of detection window, where the number of droplets per second and coalescence frequency were calculated.

For higher dispersed flow rates at 8 and 10  $\mu\text{l}/\text{min}$ , a series of 14 117 frames were recorded. As the tendency of coalescence appeared early in the the coalescence chamber, images were recorded only at the inlet of the channel. The areas of droplets increased proportionally with tendency of coalescence. Based on the frequency, the droplets were sorted into several size classes, and the number of initial size (size 1) droplets and number of two coalesced initial size droplets (size 2) were determined from a detection window with a width depending on the diameter of the studied size classes. The droplet count at the inlet was limited to droplets with circularity at 0.7 - 1 and size area at size class 1 or 2  $\pm 300 \mu\text{m}^2$ . As the same droplets would be detected several times in the frames, the actual number of droplets of both size classes was calculated from the average flow rate and droplet volume. The droplet volume was found from the mean droplet diameter in each size class, and determined from the Analyse Particle feature in ImageJ. The difference in number of size 1 and 2 was the main parameter for comparison between the different crude oil systems.

#### 5.4.5 Cleaning Procedure

After the microfluidic experiment was finished, the oil, water and outlet tubing were removed from the chip holder, and placed in waste beakers. A cleaning script was started from the software. The script included automatic flushing of water and xylene by filling and withdrawing the water syringe and oil syringe, respectively. When the syringes and tubings were cleaned properly, a manual injection of xylene into the oil syringe was performed to remove potential oil residues. Both syringes were dismounted from the flow setup, and further cleaned by toluene and acetone before they were put into a heating cabinet at 60 °C over night.

The method for cleaning the glass chips and ferrules included application of ultrasonic waves. The parts were placed in plastic cups and put into a toluene/acetone mixture (3:1 v/v), followed by cleaning of only chips in Decon 90 solution, before chips and ferrules were put into an isopropanol solution. The last cleaning step for the glass chips was in deionized water. Each step included sonication for 15 minutes. After the cleaning procedure was performed, the chips were placed in an ashing furnace at 475 °C over night. The ferrules were placed in a heating cabinet at 60 °C.

Due to problems with precipitation of unknown material in the coalescence chamber and T-junction of the glass chips during some experiments, an additional cleaning step was necessary. The procedure included cleaning with Piranha which consisted of 1 part hydrogen peroxide and 3 parts sulfuric acid by volume. The chip was reoriented during cleaning to ensure all surfaces and channels got in contact with the solution for a significant time.

## 5.5 Interfacial Tension Measurements

### 5.5.1 Experimental setup

The capillary tubes used in the interfacial tensions measurements were made of borosilicate glass with a length of 120 mm and an inner diameter of 4 mm. The interfacial measurements were performed by using a SVT 20 spinning drop video tensiometer developed by DataPhysics [90]. The experimental setup included a measuring cell, a high speed camera and a water bath for temperature control. Figure 15 shows a simplified overview of the experimental setup of the spinning drop video tensiometer.

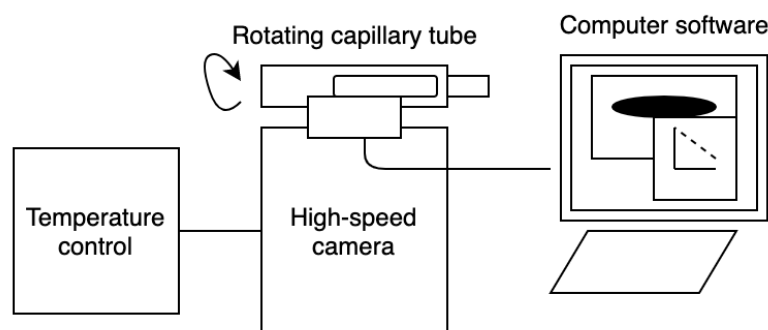


Figure 15: Experimental setup of spinning drop video tensiometer.

The structural sketch includes a camera with an ocular which detects the interfacial tension. The capillary is placed inside a holder in the measurement chamber which is illuminated by a light source [90].

### 5.5.2 Sample Preparation

The sample preparation included pre-heating of the crude oil sample at 60°C for approximately 30 minutes in a heating cabinet. A disposable pasteur pipette (230 mm) was used for injection of the water phase in the capillary. The capillary tube and the pasteur pipette were flushed with water phase before use. The filling of the capillary tube was introduced bottom-up to avoid air bubbles. The filling of water was complete when the phase shaped a bubble at the top of the capillary to ensure no air in the sample.

The injection of oil droplets was performed with a disposable syringe and a needle (0.80 x 50 mm). Oil droplets at 2-5  $\mu\text{l}$  were added into the tube. The injection of a suitable and shaped droplet was quite difficult as the crude oil was not very viscous. The droplet injection was done by small movements of the needle with contact of the capillary wall to provide release of droplet. If the capillary had lost its water bubble at the top, an additional injection of water phase was implemented.

### 5.5.3 Spinning Drop Procedure

The interfacial tension between the crude oil and water phase was measured by the spinning drop tensiometer. The three chemical demulsifiers; Brij-93, EB-8075 and Pluronic PE8100 were analyzed at 5 ppm and 25 ppm concentrations. The experiments were carried out at room temperature, at approximately 23 °C. Before running the experiment, the specific densities of the water and crude oil phase were inserted to the software (SVT20). The capillary was injected into the measuring cell. The camera position was adjusted to detect the crude oil droplet, and the rotation speed was increased to 6000 - 10 000 rpm depending on the crude oil volume, to provide elongation of droplet. Adjustments of zoom, focus, illumination and tilt functions were performed to obtain a stable and sharp droplet with contrast.

The calibration was done to obtain a reference value for the interfacial tension. The procedure was conducted at the start of each spinning drop experiment for correction of optical distortions. The calibration was implemented by camera movement by detection of the right side of the droplet at different positions. In order to perform successful calibrations, the most suitable zoom was set to be 1.0, and if the droplets tend to get relatively large it was set to 0.7. By pressing extract profile, hold drop and tracking functions in the software, a result window with measurement values gave a visualization of the interfacial tension as a function of time and camera position every five seconds. By studying the camera position, one had the possibility to monitor the droplet movement. The complete interfacial measurement lasted approximately 2 hours until the interfacial tension had been stable over a time period of approximately 15 minutes.

#### 5.5.4 Cleaning Procedure

To avoid systematic errors and contaminated samples, the preparation of samples and instrument is greatly important. After the measurement, the capillary was repeatedly cleaned with water and organic solvents such as acetone and toluene to dissolve crude oil. After flushing the capillary five times with each solvent, it was placed in a heating cabinet at 60 °C for approximately 2 hours.

## 5.6 Quartz Crystal Microbalance

### 5.6.1 Experimental Setup

The experimental QCM-D setup (QSense Explorer) delivered by Biolin Scientific included a flow module which was part of the temperature controller. As the monitored oscillation frequency got affected by temperature changes, the quartz crystal holder was placed inside the flow module. To reach set temperature, the sample liquid was lead in tubings with HPLC fittings, through a s-shaped path, before entering the surface of the sensor. A thermoelectrical device below the flow module was equipped with heating and cooling [7].

Figure 16 shows an overview of the experimental setup used in the QCM-D measurements. The tubing was arranged from the sample holder via the flow module and the peristaltic pump (Ismatec IPC-N 4). The data and signals were further generated in the electronics unit, before being sent to the Windows-based acquisition software QSoft 401. The generated data could further be analyzed in the incorporated QTools software. Physical properties of the adsorbed film layer, such as viscosity, elasticity and thickness could be extracted from the viscoelastic Voight model incorporated in the QTools software [7], [95].

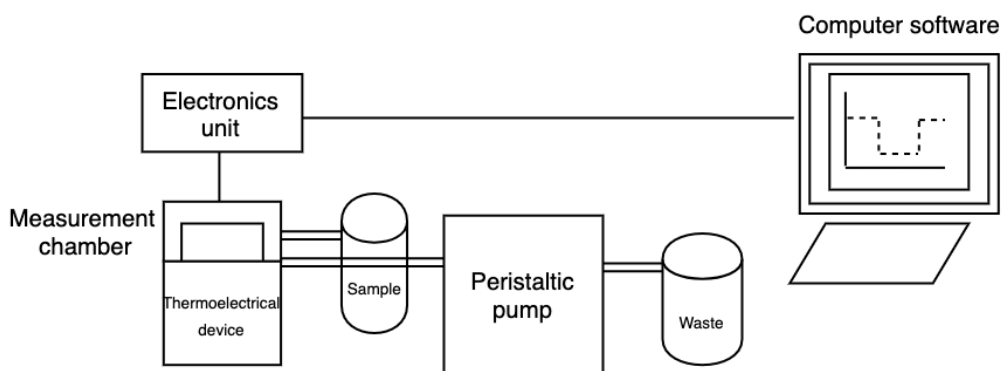


Figure 16: Experimental setup of QCM-D.



### 5.6.2 Quartz Crystal Microbalance Procedure

The silica sensor crystal was mounted, and the tubings were connected to the flow module and pump. The initial step in the QCM-D experiments was to find the resonance frequencies of the sensor crystals in the QSoft 401 software, after filling the sensor with solvent at flow conditions at 500  $\mu\text{l}/\text{min}$ . The resonances constituted the baseline signal for each crystal on the sensor, and were found in the acquisition menu below setup measurement. After finding the resonance frequencies, the pump was turned on and the experiment started.

The QCM-D experiments were performed by formation of an initial stable baseline of frequency and dissipation of xylene. As the measured  $f$  and  $D$  values are analyzed relative the values of a clean sensor, the initial step of the measurement was to establish reference values for frequency and dissipation by using solvent. When the reference values had been stable for approximately 15 minutes, the injection of pre-heated crude oil sample was performed. After approximately 30 minutes, the frequency became stable, and the second solvent injection was implemented. A final stable baseline became present after approximately 15 minutes. In addition to the original crude oil system, crude oil samples with a chemical demulsifier concentration at 25 ppm were analyzed, included xylene with a chemical demulsifier at 25 ppm. The experiments were carried out at room temperature, at approximately 23  $^{\circ}\text{C}$ . All the generated data for the experiments were analyzed in the QTools software.

### 5.6.3 Cleaning Procedure

The cleaning procedure included flushing of xylene through the flow module and the pump before the sensor was removed. Methanol was thereafter flushed. The tubings were further flushed with air to obtain dry channels for next experiment. The tubings were disconnected and the sensor removed before the visible parts of the module interior located close to the sensor holder were dried with nitrogen gas.

The sensors were cleaned with sodium dodecyl sulfate (SDS) for approximately 30 minutes before they were flushed with deionized water, dried with nitrogen gas and put into ultraviolet (UV) radiation for 15 minutes.

## 6 Results and Discussion

### 6.1 Interfacial Tension Measurements

To establish information about the adsorption of chemical demulsifier material at the interface between the oil and water phases, the interfacial tension was measured over a time period. The interfacial tension measurements were performed with crude oil samples with chemical demulsifier concentrations at 5 and 25 ppm. Figure 17 shows an overview of the IFT results for each system compared to the original system without a chemical additive. The figure shows how the IFT changes as a function of time, until it reaches an equilibrium value.

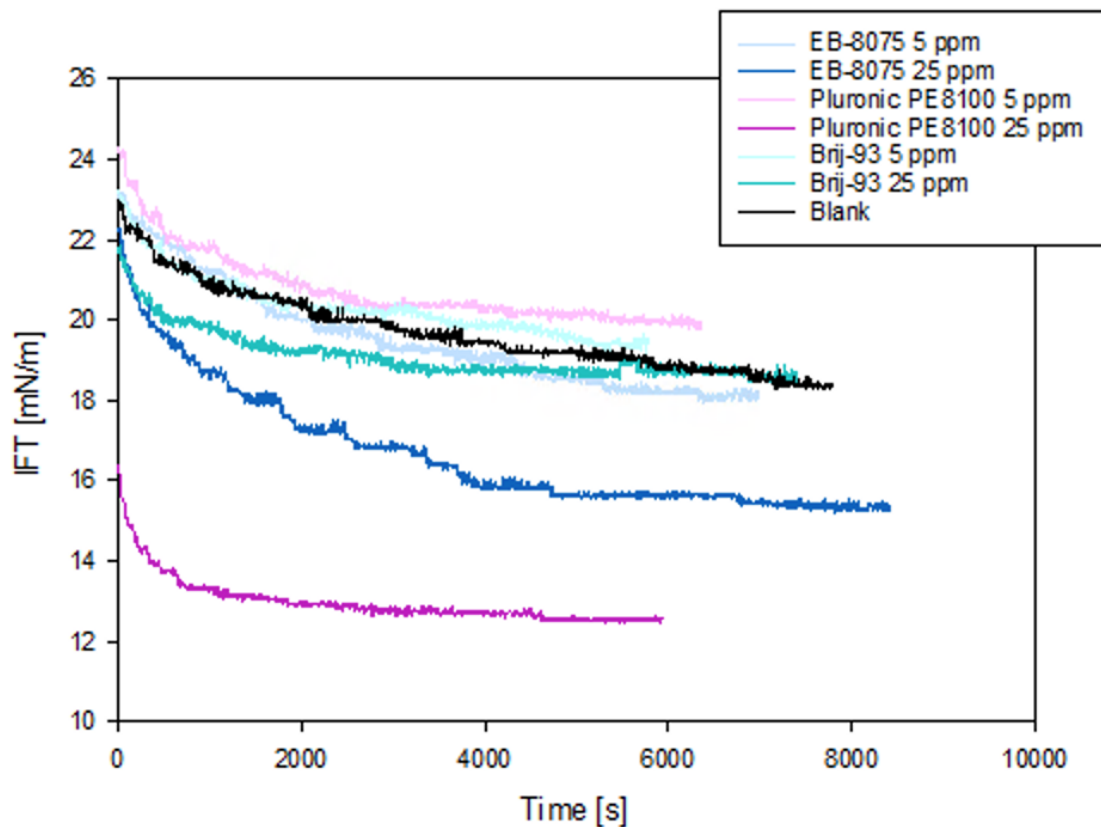


Figure 17: IFT vs. time for demulsifier solutions in crude oil at 5 and 25 ppm.

Figure 18 shows a comparison between the constant IFT values for each system. The equilibrium value was calculated from the 200 last measurement points which posed approximately the last 15 minutes of the measurement.

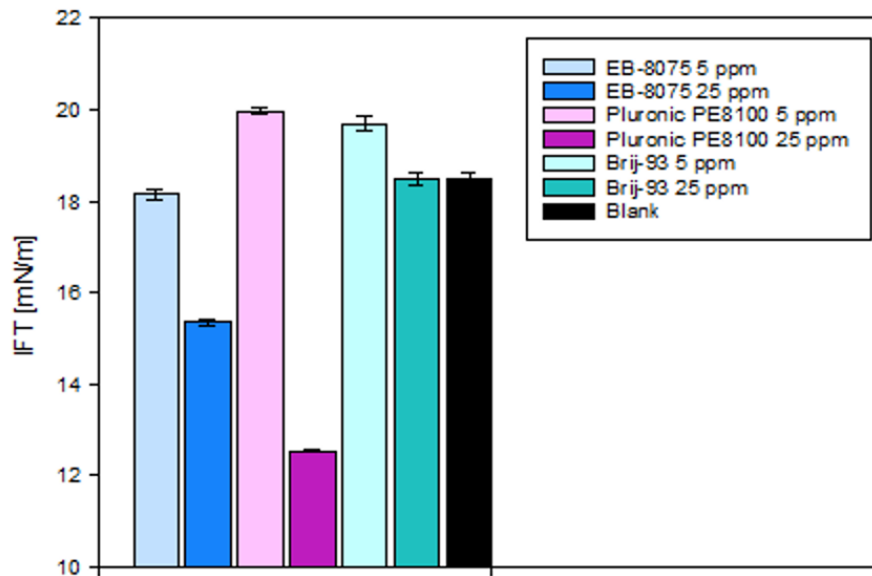


Figure 18: Equilibrium IFT values for demulsifier solutions in crude oil at 5 and 25 ppm.

The results show how an increased adsorption time of surfactant gives decreased IFT for all crude oil systems, before an equilibrium value is reached. A significant trend for all systems, is the reduction in IFT for solutions with highest demulsifier concentration at 25 ppm. The results signify that the high-molecular weight wetting agent Pluronic PE8100 provides a fast decline with a low and rapid relaxation of IFT equilibrium for the demulsifier solution at 25 ppm. As the dosage of chemical demulsifier depends on molecular weight, it was expected that Pluronic PE8100 would provide a higher reduction in IFT compared to Brij-93. The former chemical demulsifier has a 6 times higher molecular weight than Brij-93 [10].

Pluronic PE8100 type is a common wetting agent due to its polyoxyethylene chains which have proven to be very hydrophilic. Even though the Brij-93 has a higher HLB value, it has a significantly lower molecular weight than Pluronic PE8100 [11]. Which claims that an equal dosage of these chemicals, leads to different reductions in IFT, which is reflected in the results.

Considering the systems with Brij-93, the results show that an increase in chemical demulsifier concentration from 5 ppm to 25 ppm, gives the smallest reduction in IFT, compared to the other systems. It may be assumed that the system probably will reach a fully occupied interface upon an even small increase in concentration.

The occupation of adsorbed surface-active components on the interface might affect several rheological properties of the surfactant, such as the interfacial tension, as it will reach a constant IFT value. Considering Brij-93 and Pluronic at 25 ppm, the system shows the most rapid time to reach equilibrium. Compared to EB-8075 at 25 ppm, the IFT behaviour is not similar, as the increase in chemical demulsifier concentration gives a rather slow but significant reduction in IFT. The slow reduction may indicate a relatively high adsorption time of demulsifier concentration.

According to the interfacial tension values for the 5 ppm systems, they have insignificant deviations from the original system without a chemical additive. Considering the chemical dosage, the systems do apparently demand higher demulsifier concentration to obtain changes in interfacial tension for such systems. It is still worth mentioning that the Brij-93 and Pluronic systems at 5 ppm show a small increase in IFT compared to the original system without a chemical demulsifier. The deviations might be due to desorption of demulsifier molecules at the interface or deformation of the cylindrical shaped droplet.

Based on the Young-Laplace equation for calculation of IFT, the value is depending on the angular velocity of the capillary, the radius of the cylindrical shaped droplet and the density difference between the two phases [6]. The higher IFT values for 5 ppm solutions of Brij-93 and Pluronic PE8100 may therefore be caused by unequal angular velocity during droplet formation. During experiment, it was impossible to use similar rotational speed due to different sample volumes. As the crude oil is quite light with a density at  $0.846 \text{ g/cm}^3$ , the injection of an optimum crude oil volume was rather difficult. The different sample volumes caused unsimilar droplet shapes with unequal droplet radius. The longer cylindrical shape, the larger radius which will provide less surface tensions resistance. Hence, a lower interfacial tension. This might be assumed to be a source of error for certain experiments where the IFT value is higher than the system without added demulsifier. The experiments involved other sources of error, such as occurrence of air bubbles which probably could affect the IFT during measurement. If the air bubble was small and located at a distance far from the actual oil droplet, and did not get in contact with the droplet, they were ignored. In certain experiments where air bubbles occurred and got in contact with the oil droplet, it led to a decrease in IFT. To prevent disturbed IFT signals, the tilt angle was adjusted and the rotational speed was quickly increased before decreased. The quick variation of the angular velocity was to prevent droplet deformation, hence fluctuations in IFT.

## 6.2 Quartz Crystal Microbalance

The initial QCM measurements were performed with crude oil samples with a chemical demulsifier concentration at 25 ppm. The main results from the measurements were adsorbed mass as a function of frequency. The calculation of adsorbed mass was based on the establishment of a baseline from xylene injection to find reference values for frequency and dissipation. After a stable baseline was created, the injection of crude oil sample was performed before a final addition of xylene. The relative change in frequency between the first and second injection of solvent was used in the calculation of adsorbed mass. Figure 19 shows the results of frequency behaviour as a function of time for QCM analysis of crude oil systems. The figure shows the behaviour for the original crude oil without demulsifier (blank) included the systems with Brij-93, EB-8075 and Pluronic PE8100.

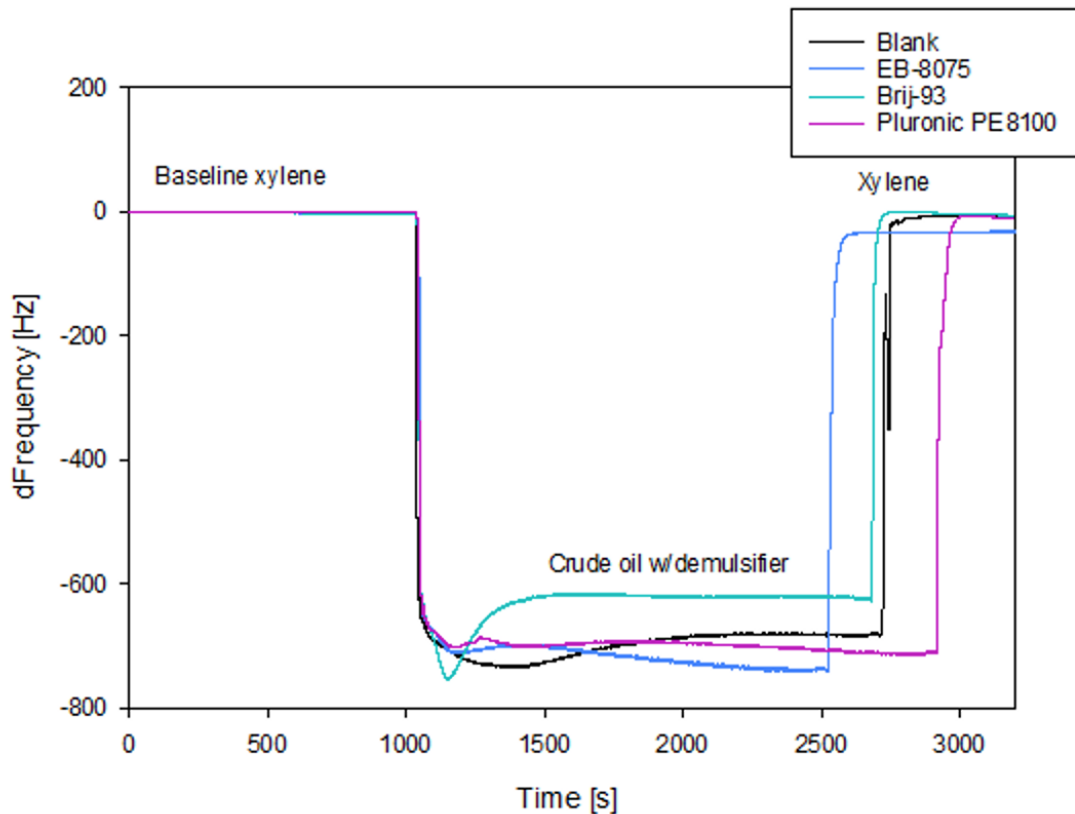


Figure 19: Frequency change for demulsifiers in crude oil.

Figure 19 does not show large deviations for the different systems. The EB-8075 demulsifier system presents the most significant change in frequency, as the frequency after the second injection of xylene stabilizes at the lowest value. The plot does also signify that Brij-93 obtain the lowest change in frequency during crude oil injection, hence the lowest coupled mass on the quartz sensor. The results show a change after injection of crude oil and demulsifier for all systems. The fast decrease of frequency is assumed to be a result of fast adsorption of material on the surface or change in density and viscosity of the fluid. For all systems, except Brij-93 and the original system without demulsifier (blank), the frequency stabilizes almost instantly at approximately -700 Hz. The increased frequency behaviour for the Brij-93 and blank system may be caused by a rather fast adsorption of molecules. When they have reached the surface, they will probably organize themselves on the layer to form a packed layer structure. The packing may lead to release of water which is reflected of the increasing frequency.

The QCM-D technique based on the energy dissipation monitored the spreading behaviour and viscoelastic properties of the adsorbed material on the sensor surface. The dissipation change is shown in Figure 20.

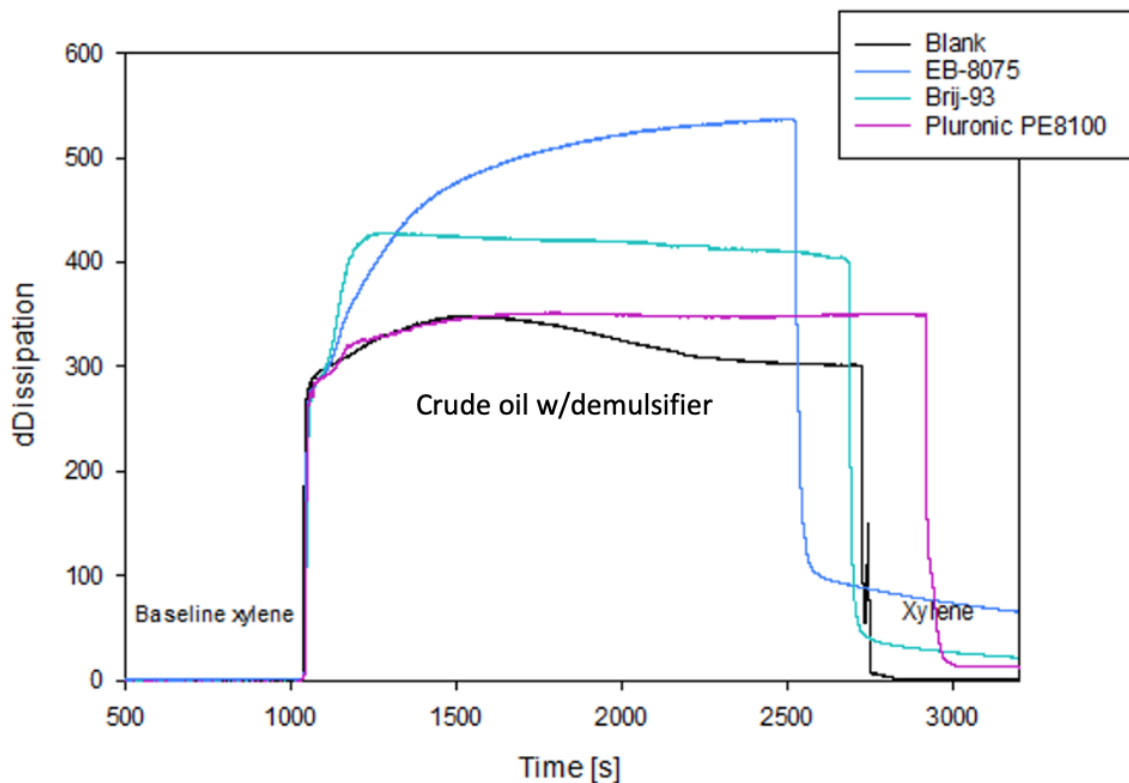


Figure 20: Dissipation change for demulsifiers in crude oil.

Based on the results, one can see how the EB-8075 demulsifier shows a great increase in dissipation. The high dissipation reflects formation of a soft and viscoelastic adsorbed layer. While the blank and Brij-93 show a rather simultaneous behaviour where the dissipation presents a rather fast increase before the dissipation decreases due to probably a small water release. In general, systems which contained blank, Brij-93 and Pluronic PE8100 provide a more rigid layer compared to the system which include the chemical demulsifier EB-8075. Considering the latter system, the change in dissipation does seem to stabilize slower compared to the other systems. The dissipation is an additional measure used to obtain additional information and visualization about the physical properties of the adsorbed layer. Including an imagination of the reorganization of adsorbed molecules on the surface. Based on the results, the Pluronic PE8100 does not undergo any significant structural changes during measurement as the dissipation reaches a quite stable dissipation value at approximately 300 rather fast.

The QCM-D measurements did also include measurements of chemical demulsifiers with a concentration at 25 ppm dissolved in only xylene. The additional tests were performed to obtain information about the contribution of only demulsifier in the crude oil/demulsifier adsorption phenomena. Figure 21 shows the change in frequency and dissipation for all demulsifiers.

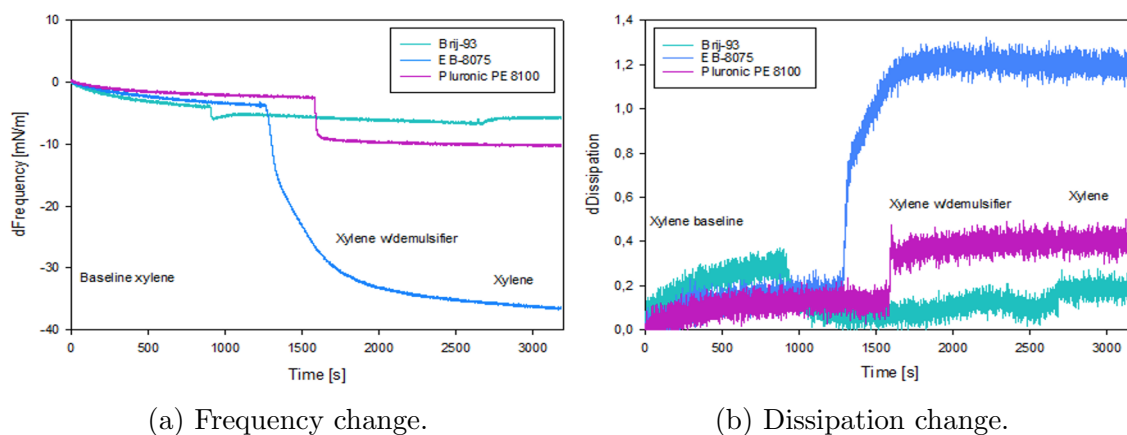


Figure 21: Frequency and dissipation change for demulsifiers in xylene.

By comparing the xylene and demulsifier systems in Figure 21a, with the crude oil and demulsifier systems, a significant variation is the much lower overall change in frequency. It indicates that the high decrease in frequency for the crude oil systems was caused by the crude oil. Brij-93 show a quite similar behaviour compared to the system with crude oil. As the behaviour of frequency experiences a rather steep decrease before it undergoes an increase and stabilizes. The demulsifier will probably affect the organization of molecules, and facilitate release of water from the crystal

surface. The Pluronic PE8100 demulsifier shows a rather different behaviour of frequency, as it stabilizes once the injection of xylene and demulsifier was performed. This demulsifier does also provide a higher total change in frequency compared to Brij-93. One can also assume that the EB-8075 demulsifier presents the most effective component for adsorption on the hydrophilic silica surface as the overall change in frequency after the second injection of xylene is not visible.

Figure 21b shows that the change in dissipation for systems with xylene and demulsifier provide much smaller fluctuations of dissipation signals compared to the systems with crude oil. Hence, the results indicate that the elasticity, viscosity and density of the adsorbed layer are clearly lower without crude oil. Therefore, the presence of crude oil in a demulsifier solution will contribute to a significantly higher adsorption to the crystal surface.

According to Figure 21a and 21b, it is worth mentioning the unstable initial baseline of xylene. The problem solving included elimination of all factors which induced uncontrolled and unwanted changes in the measured parameters. Air bubbles were eliminated by stopping the pump during change of sample injection, temperature changes were monitored by the temperature controller, bad electrical contacts were checked and possible solvent leakages were stopped.

Another reason for the instability, was unanticipated surface reactions or back-side reactions which took place between the sensor coating and the xylene. The internal interaction might be due to dissolving or swelling on the surface, which was reflected in the unstable frequency and dissipation for the initial injection of xylene. As the error was present for the majority of the measurements, the problem which tended to be a baseline drift was probably an unavoidable consequence of either the experimental setup or the selection of xylene as a solvent. As these factors induced measurable changes in frequency and dissipation, they distort the actual measurement of the physical adsorption process. Therefore, the calculation of adsorbed mass on the surface would get reduced by the negative frequency of the baseline. The calculated values based on Sauerbrey equation for adsorbed mass for all systems are shown in Figure 22.



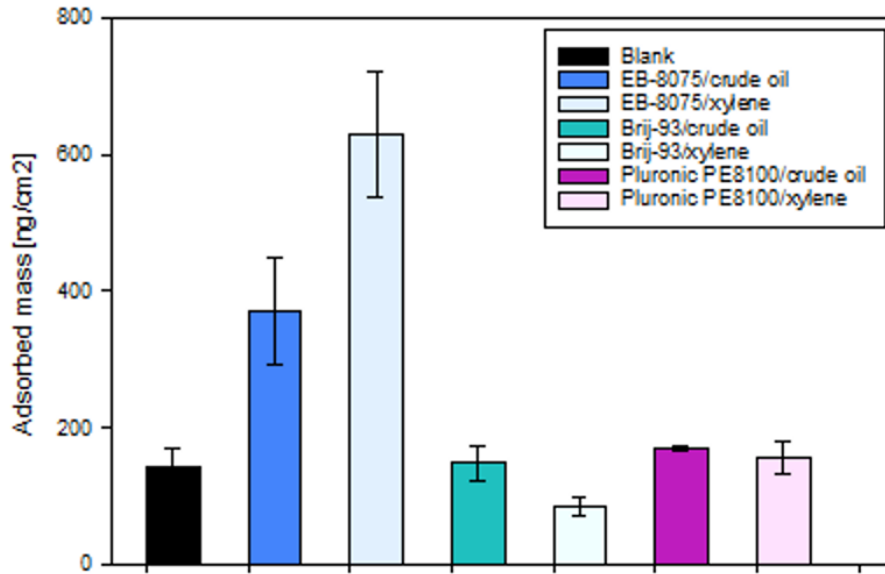


Figure 22: Adsorbed mass for xylene/demulsifier and crude oil/demulsifier.

Table 3 shows the thickness of film layer based on adsorbed mass.

Table 3: Film layer thickness.

	Layer thickness [nm]
Blank	1.71
EB-8075/crude oil	4.39
EB-8075/xylene	7.43
Brij-93/crude oil	1.76
Brij-93/xylene	1.00
Pluronic PE8100/crude oil	2.68
Pluronic PE8100/xylene	1.85

The calculation of film layer thickness is based on the assumption of no solvent on the surface. The assumption is probably not valid, as the surface will contain residues of solvent. Especially if the occurrence of unanticipated surface reactions of the surface coating and solvent are present. The film layer thickness will therefore only give a basis for comparison of the different demulsifiers.

The calculation of adsorbed mass is based on three parallels of each sample solution. The results show that the solution with EB-8075 dissolved in crude oil gave significantly lower amount of adsorbed material at  $371 \text{ ng/cm}^2$ , compared to the system with EB-8075 demulsifier dissolved in xylene with an adsorbed mass at

628 ng/cm<sup>2</sup>. The values provide information about a mixed surface of both crude oil components and demulsifier. As the adsorption is much higher for the system without crude oil, it can be assumed that chemical interactions between crude oil components and demulsifier molecules have taken place. Hence, the crude oil will probably prevent adsorption of demulsifier at the surface for this system.

According to the calculation of adsorbed mass for the Brij-93 systems, the solution of demulsifier dissolved in crude oil shows a greater adsorption at 149 ng/cm<sup>2</sup> compared to the xylene solution at 85 ng/cm<sup>2</sup>. For such systems, the crude oil will probably facilitate adsorption of demulsifier and allow a mixed surface. On the other hand, by comparison of the original crude oil system without demulsifier with an adsorbed mass at 146 ng/cm<sup>2</sup> and the crude oil system with Brij-93, it will indicate that almost all adsorbed material is constituted by crude oil components.

The Pluronic PE8100 system gives a relatively low adsorbed mass at 171 ng/cm<sup>2</sup> for the crude oil solution, and 157 ng/cm<sup>2</sup> for the xylene solution. A comparison between these measurements, indicates a great adsorption of demulsifier. When it comes to the crude oil system, it shows a similar adsorption of mass compared to the original system without demulsifier. Based on the results, the QCM-D measurements do not give a clear indication to assess the property of adsorption for demulsifiers. Certain systems provide different impacts on the sensor which might be interpreted differently.

Considering the overall comparison between the different demulsifiers, the molecular weight of Pluronic PE8100 at 2300 g/mol probably causes higher adsorption compared to Brij-93 with a molecular weight at 357 g/mol. Even though the latter demulsifier has a higher HLB value, it has a significantly lower molecular weight which probably has a greater effect on the adsorption.

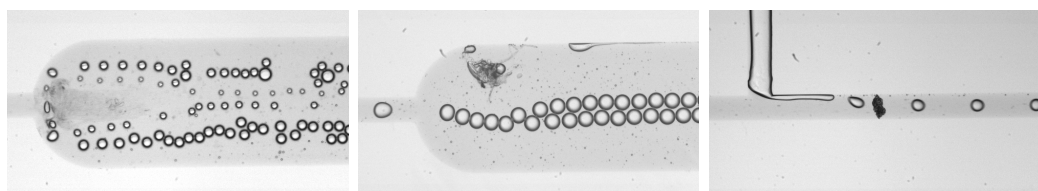
Comparing the QCM-D measurements with the IFT results, one can notice a large relative change in frequency and dissipation for the EB-8075 system compared to the other demulsifier systems. The EB-8075 provided a slow, but high reduction in IFT which is reflected in the change in frequency and dissipation from the QCM-D measurements. The EB-8075 demulsifier does apparently give a significantly high behaviour of adsorption which is obtained much slower compared to the Pluronic PE8100 system. The steep decrease of IFT for Pluronic PE8100 at 25 ppm is clearly visualized also in the rapid change of frequency and dissipation before obtaining equilibrium values for both parameters.

## 6.3 Microfluidic Measurements

### 6.3.1 Method Development

The microfluidic experiments involved tests of parameters such as temperature and flow rates of continuous and dispersed phases. During the tests, several problems arised due to non-ideal facilitation for W/O systems. As W/O systems include high content of crude oil compared to O/W systems, unexpected situations related to pressure changes, precipitation of particles and coating problems were present. Therefore, modifications of the setup and procedure were conducted to implement optimized experimental conditions for the W/O experiments. One of the main problems related to the continuous oil flow, was leakage from the syringe plunger at maximum filling of crude oil. One of the possible improvements was the selection of a stainless steel syringe. As the syringe included a temperature controller, it was possible to perform temperature tests. Another solution was to replace it with a tighter plunger. The replacement seemed to work as the tests did not experience more leakage.

During the flow rate tests, detection of precipitation in the microchannels and adsorption on glass surfaces of unknown materials were present. Example of the detected particles are shown in Figure 23. The problem created errors in droplet generation and flow behaviour in the coalescence chamber. It was assumed to be either heavy components from the crude oil, fibres from degradation of o-ring swelling or airborne dust particles. To avoid possible depositions of crude oil components which could prevent optimal droplet generation and detection, the initial experimental step involved preheating of crude oil samples to homogenize the solution. Even though the procedure included preheating, the precipitation still occurred.



(a) Droplet generation disturbance. (b) Water flow disturbance at inlet. (c) Blockage in meandering channel.

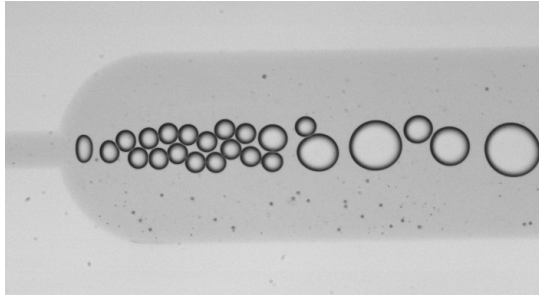
Figure 23: Detected particles in flow channels.

Other related problems caused by precipitation of material, were the increased pressure of the system which exceeded the pressure limit at about 10 bar. As a result of this, the inlet tubings of the microfluidic chips underwent leakage on the chip surfaces which caused blurry microscopic images and non-favorable conditions for the microscopic objective.

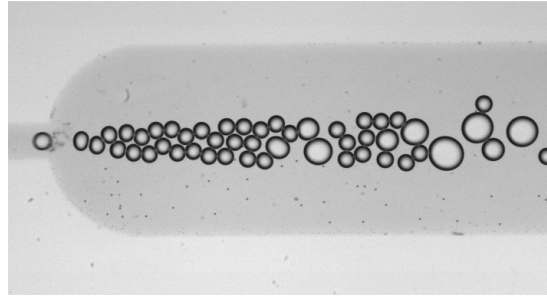
A Piranha solution was required as an additional cleaning step to purify the channel, and selection of other spare parts for the flow setup became necessary to prevent depositions. Tighter ferrules, tubings with a larger inner diameter and other chip designs with larger coalescence chambers were implemented as well. Adjustments of dispersed and continuous flow rates to maximum 100  $\mu\text{l}/\text{min}$  were performed to force the blockage to the outlet. The modifications seemed to work, as the droplet generation and flow behaviour provided expected droplet flow conditions for the W/O systems.

As the W/O systems demanded hydrophobic coating of the silica-based microfluidic glass chips, the general procedure involved an additional initial pretreatment step. The coating caused significant disturbances in the droplet generation for several measurements. For the dispersed flow tests at 8 and 10  $\mu\text{l}/\text{min}$ , the hydrophobic coating provided high fluctuations of initial droplet sizes for similar systems as shown in Figure 24a and 24b.

The OTS in toluene solution provided weak hydrophobic surfaces which tended to act almost as hydrophilic. New hydrophobic coating solutions were prepared, which worked relatively well until solution aging became apparent probably due to hydrolysis and polymerization of the OTS solution. Modified coating procedures were developed to improve the hydrophobicity. The standard coating procedure involved injection of coating solution in 15 minutes before drying. The improved procedures included an injection time at 10 minutes followed by a second injection at 10 minutes. A third coating procedure was performed by filling the solution in 45 minutes before drying. The weakened hydrophobic strength was possibly caused by breakage of the covalently bonded siloxane groups on the surface, which may have been caused by interaction with particles from a crumbled cap on the OTS solution bottle. Figure 24c shows an example of a well established hydrophobic coating compared to an unsuccessful coating layer at the T-junction for crude oil and water phase in the microfluidic chip shown in Figure 24d.



(a) Normal initial droplet sizes.



(b) Small initial droplet sizes.



(c) Hydrophobic coating.



(d) No hydrophobic coating.

Figure 24: Problems with hydrophobic coating and generation of initial droplet sizes.

### 6.3.2 3D-Printed Chips

An important objective in the microfluidic study was to perform transparent 3D printing of thermoplastic materials of varying degrees of translucency. Figure 25 shows several 3D-print results.

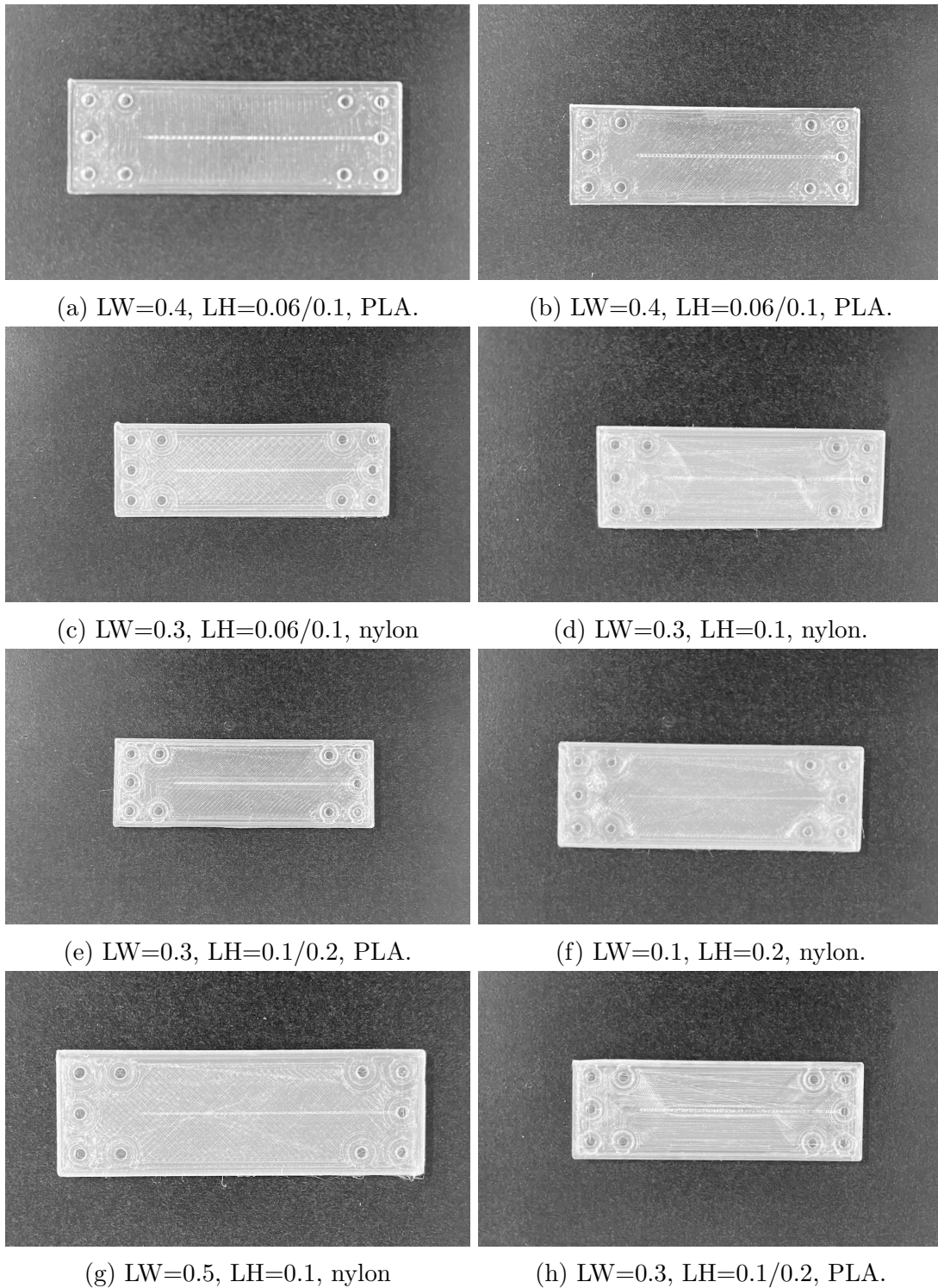


Figure 25: Problems with hydrophobic coating and generation of initial droplet sizes.



The printing was done with chip design 2 visualized in section 5.4.2. The printing included testing of two thermoplastic materials; nylon and polyactic acid (PLA). In addition to selection of material, different pattern prints were tested. The print settings involved different layer heights (LH) and line widths (LW). The transparency of the chips was adjusted by varying these parameters included infill density, support and print speed.

The chips shown in Figure 25a and 25b are printed with similar print settings and material, but differ due to print type as the line angles are set to [0.0] and [45.45], respectively. A comparison shows that the latter one which includes a obliquely pattern print does provide a higher refraction of light, hence a more translucent print [96].

By studying Figure 25c and 25d, one can see that the print pattern does have a significant impact on the transparency of the print. Both chips are printed in nylon and with similar line width and layer height, but every other layer is printed in a cross-pattern for the former chip. The printed chip shown in Figure 25d includes a concentric pattern where every other layer is printed vertical and horizontal. The degree of transparency is apparently depending on the geometry. Complex geometries do tend to refract light more. Therefore, it is less likely to obtain clear prints. Considering the results, a concentric print pattern provides lower transparency as the geometry becomes more complex and the horizontal lines have a tendency to obscure the main coalescence chamber in the channel configuration. The same trend is also shown for the chip in Figure 25h printed in PLA.

Considering how the print settings such as the layer height affect the transparency, the chip shown in Figure 25f has the highest layer height, and seems to provide a translucent print. According to the result, it is probably favorable with thin layer heights, as thick layers have a tendency to disperse more light. It seems like the dispersion redirects the light and causes an opaque appearance of the channel configuration [96]. In addition to minimization of light refraction, a low layer height provides high print precision which is highly preferred.

Considering the line width, a small width demands a higher number of print line directions. A large number of print line directions probably causes a high refraction which is non-favorable. Therefore, high line width provides a transparent appearance which is shown in Figure 25a. The chip shown in Figure 25g includes the highest line width, but the cross-pattern seemingly decreases the tendency of transparency. The effect of line width should be further assessed by testing different widths with similar print types to obtain sufficient comparable prints.

As the print shown in Figure 25a had the best transparency, it was tested in the microfluidic setup, and Figure 26 shows snapshots from the testing with the 3D-printed chip design.

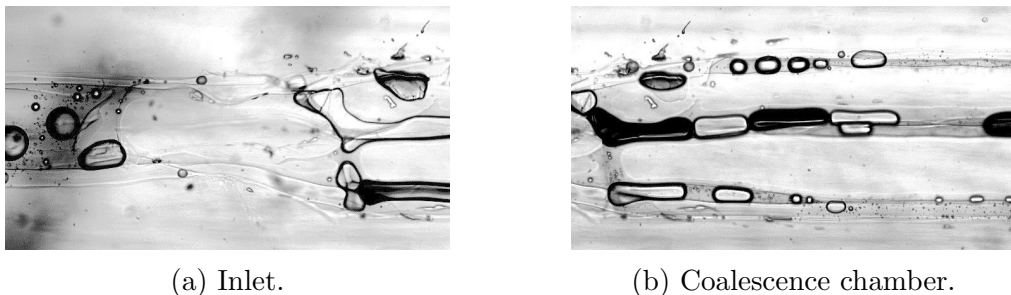


Figure 26: 3D-printed chip design 2.

Figure 26a shows the connection point located between the meandering channel and the coalescence chamber. As water had the lowest viscosity, it was forced through the channel with a pressure exceeding maximum threshold. Figure 26b shows a better overview of the liquid fractions which actually reached the chamber. The main part of the droplets was probably air bubbles which may originated from the relatively low infill density which was used in the printing. One can also detect the not uniform channels which lead to non-continuous flow. As the chip dimensions were given in micrometers, the 3D-printer did probably not have an optimal resolution for such small-scale prints.

The chips were printed with the bottom plate lying on the print surface. As the print creates a support structure during printing, an alternative way to print could be to reorganize the chip to stand. Hence, the print direction would circulate around the channels. As the microfluidic tests involve relatively high pressure, it might be possible to avoid leakage of fluid by print one of the short sides first. It would probably increase the strength and resistance against flow. It is difficult to predict the transparency of such prints, but post-treatment by polishing would probably cause smoother surfaces.

As the microfluidic experiments with the 3D-printed chip did not provide sufficient performance, the custom-made glass chips were used in the main microfluidic tests.



### 6.3.3 Modification of Method

#### Glass Chip Design

The microfluidic method development included modifications of the actual procedure. Due to the significant problem related to clogging of the meandering and coalescence channel, the testing of different glass chip designs became a necessary step to provide valuable information about the W/O system [8]. The design tests included experiments with four different coalescence chips shown in Figure 27.

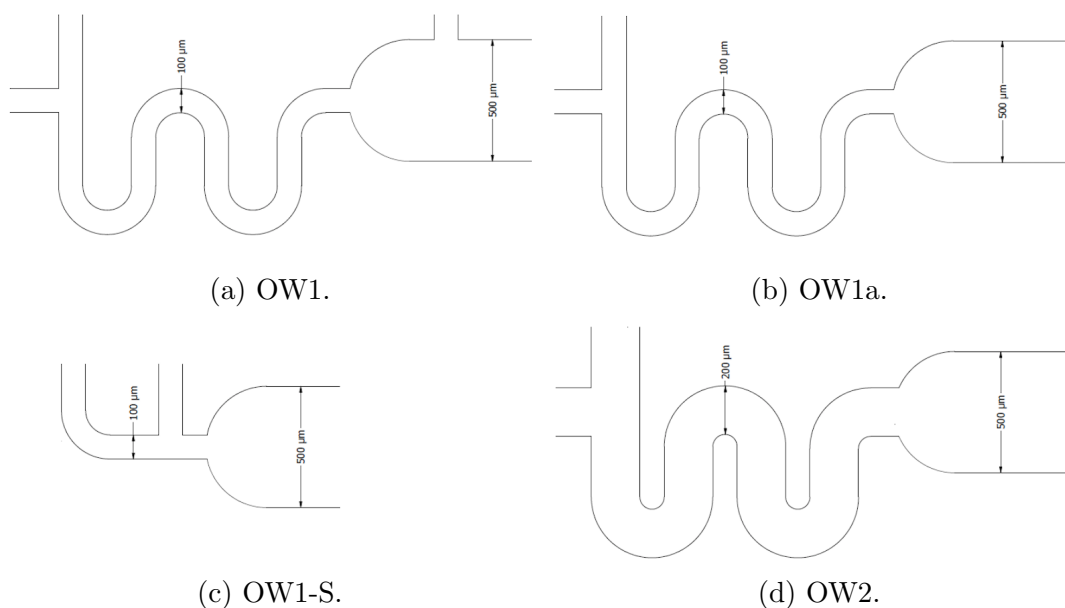


Figure 27: Chip designs with different channel configurations.

Chip design OW1 gave similar flow behaviour as the standard chip design OW1a, at equal flow rates of continuous and dispersed phase. During usage of OW1 with an additional oil flow inlet located directly in the coalescence chamber, this inlet was blocked to obtain only one oil inlet located above the T-junction. The OW1 chip design were used in addition to OW1a to be able to perform unlimited number of tests.

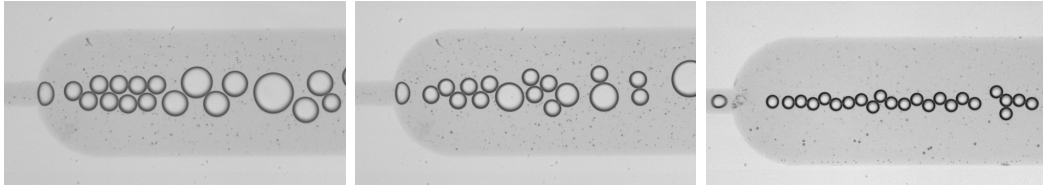
Chip design OW1-S involved a singular meandering channel for droplet aging. To maintain a continuous flow of oil and water phase without blockage due to fibres or other unknown materials, tests with chip design which included less meandered channels, lower pressure and lower droplet aging were necessary to examine. The resulting flow behaviour indicated very high coalescence frequency which did not fit the preferred level of coalescence for further measurements with demulsifiers.

Chip design OW2 included wider meandering channels at the inlet part. As a consequence, the flow rate of continuous oil phase had to be increased 1/3 of the set flow rate determined in the continuous flow rate tests. The high oil flow was non-favorable due to high amounts of sample volumes, large drop size distributions in the coalescence chamber and high system pressure. Due to unfavorable flow conditions when using chip design OW1-S and OW2, chip design OW1a was used in the further microfluidic tests.

## Continuous Flow Rate Tests

The continuous flow rate tests included adjustments of flow rates from 40 to 80  $\mu\text{l}/\text{min}$  of the crude oil without demulsifier, to establish an indication of a preferred oil flow rate for further testing with demulsifiers. The results showed that flow rates at 40 and 50  $\mu\text{l}/\text{min}$  gave significantly high coalescence frequency which resulted in difficult image analysis for detection of tendency of coalescence, and a non-favorable reference state for demulsifier tests.

On the other hand, higher oil flow rates at 60, 70 and 80  $\mu\text{l}/\text{min}$  gave more preferred continuous flow conditions, as the tests implied relatively low coalescence frequency and a favorable water droplet flow at dispersed rates from 3 to 5  $\mu\text{l}/\text{min}$ . Figure 28 shows the inlet of the coalescence chamber with a dispersed flow rate at 4  $\mu\text{l}/\text{min}$  and a continuous flow rate at 40, 50 and 80  $\mu\text{l}/\text{min}$ , respectively.



(a) Continuous oil flow at 40  $\mu\text{l}/\text{min}$ .

(b) Continuous oil flow at 50  $\mu\text{l}/\text{min}$ .

(c) Continuous oil flow at 80  $\mu\text{l}/\text{min}$

Figure 28: Water flow behaviour from the continuous oil flow tests.

Figure 28a and 28b indicate that a relatively small increase in continuous flow rate give a significantly lower tendency of droplet coalescence for low dispersed flow rates. Figure 28c shows that a continuous flow rate at 80  $\mu\text{l}/\text{min}$  gives a well established droplet flow of initially created droplets without any coalescence present at the inlet. This was the favorable droplet behaviour for further testing of dispersed flow rates.

The results from the continuous oil flow rate tests show that an adjustment of the continuous oil flow rate does have an effect on the droplet and size distribution of the system. If the continuous flow rate is relatively high compared to the dispersed flow rate, the water droplets will maintain small at a size distribution similar to the initially generated droplet sizes. On the other hand, a low continuous flow rate causes a high water fraction which enhance growth of bigger droplets. Despite that the calculated tendency of frequency was quite good, the droplet count per second involved high variations. It was assumed that the main contribution to the disturbances was probably recordings of the same droplet object in the same frame. By reviewing the results, it was decided to continue the microfluidic experiments with a continuous oil flow rate at 80  $\mu\text{l}/\text{min}$  for further testing.

## Dispersed Flow Rate Tests

The dispersed flow rate tests included adjustments of flow rates from 3 to 10  $\mu\text{l}/\text{min}$  of the water phase, to study how the coalescence behaviour for the different demulsifier systems would be affected. In other words, how the droplet size distribution would change by increasing the volume rate of water gradually. The 8 and 10  $\mu\text{l}/\text{min}$  rates contribute to the main results, and will be presented in a separate section. Considering the tests performed with 3 and 4  $\mu\text{l}/\text{min}$ , it included experiments with the three demulsifiers with a concentration at 5 and 25 ppm. The results from the dispersed flow rate tests are shown in Figure 29.

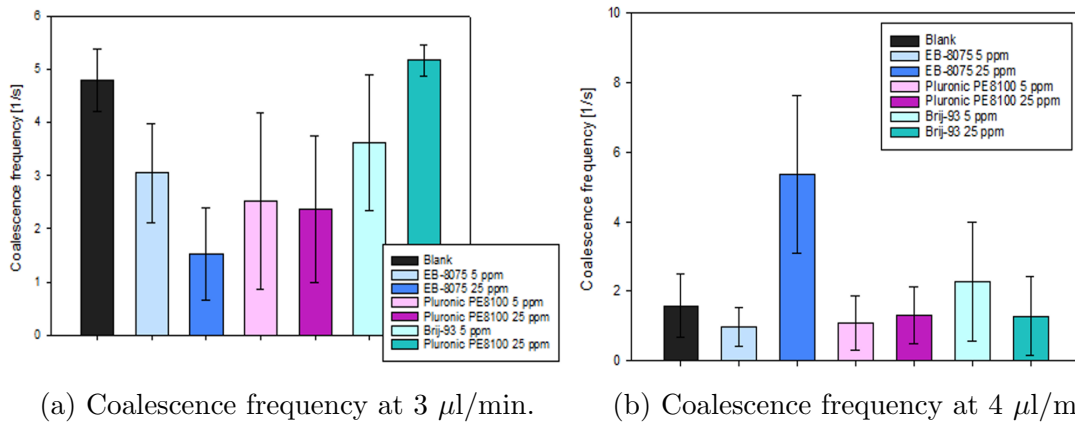


Figure 29: Coalescence frequency for dispersed flow rate tests at 3 and 4  $\mu\text{l}/\text{min}$ .

Considering the results for the low dispersed flow rates, they do not reflect the results from the bottle tests. There might be several reasons for the results, such as disturbances in droplet count. The droplet count at the outlet of the coalescence chamber is performed by using a relatively wide detection window in the ImageJ for droplet counting, which encounter the possibility for duplicates of the counting of same droplet. By studying several frames, the same droplet was counted up to 11 times in the same recording which gave rise to enormous errors related to counting. An increase in frame rate would probably decrease the errors related to recording of same objects several times. The tests did also signify larger number of droplets per second for lower flow rates, which does not indicate trustable results.

Considering the tendency to undergo coalescence for the different demulsifiers, they show significantly low efficiency. The systems with chemical additives show an even lower coalescence frequency compared to the original crude oil system without demulsifier. As the efficiency of the demulsifiers had been examined earlier related to surface activity and phase separation through interfacial tension measurements and bottle tests [97], it was clear that the results expressed high deviations due

to fluctuations in flow behaviour, unexpected pressure changes and other problems related to the flow setup for the W/O system. The water flow rate was increased even higher to examine the flow behaviour at high volume flows of the water phase. The results for 8 and 10  $\mu\text{l}/\text{min}$  flow rates are presented in section 6.3.4, and contribute to the main results.

## Temperature Tests

Temperature tests were implemented to avoid problems related to depositions from the continuous crude oil phase. The temperature tests were performed with a temperature controlled steel syringe adjusted from 30 - 60 °C. The coalescence frequency for the original crude oil system without demulsifier at dispersed flow rates at 3 and 4  $\mu\text{l}/\text{min}$  is shown in Figure 30.

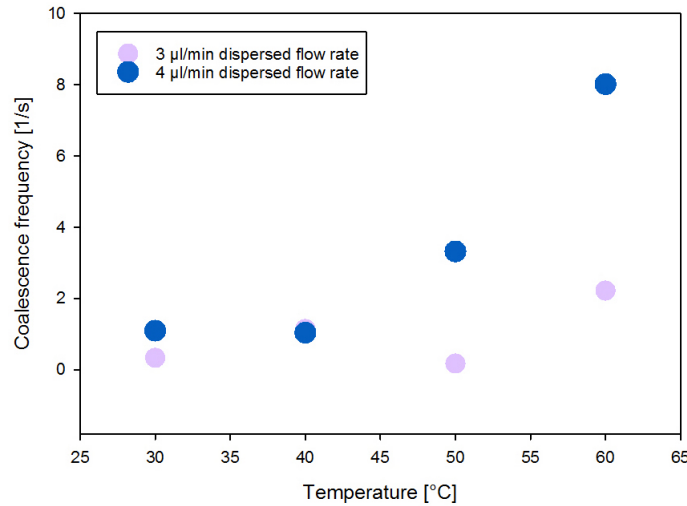


Figure 30: Coalescence frequency for a given temperature range.

The results indicate that an increase in temperature provide a higher coalescence frequency. According to the contribution of thermal energy to a demulsification process, high temperature causes reduction of the viscoelastic properties of the crude oil phase, hence a higher probability for collisions of water droplets in W/O emulsions due to a weakened interfacial film. Considering the flow rates at 3 and 4  $\mu\text{l}/\text{min}$ , it was expected that the highest dispersed phase would provide higher tendency of coalescence due to a higher water volume.

The similar trend for addition of thermal energy was also shown for tests with higher dispersed flow rates at 8 and 10  $\mu\text{l}/\text{min}$ . An increase in temperature gave a significantly higher droplet coalescence by an increase from ambient temperature conditions to 45 °C. The temperature dependent tests are shown in Figure 31. As the ambient temperature tests included the smallest droplet size distributions, the further microfluidic tests were performed at room temperature.

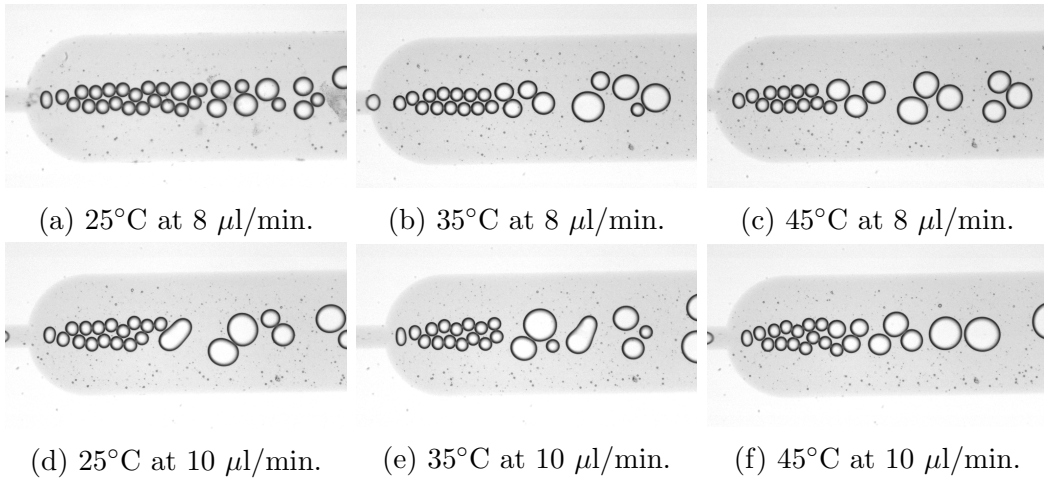
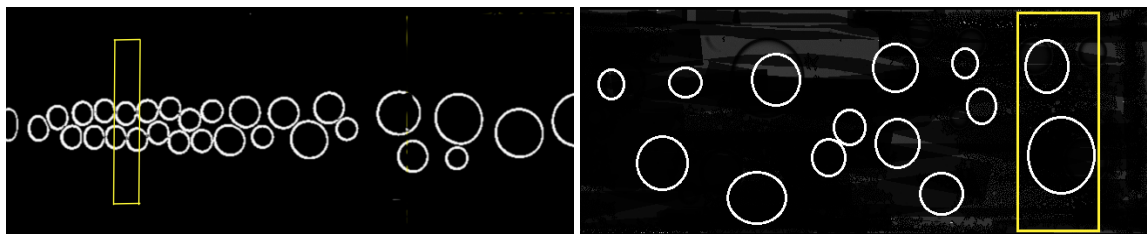


Figure 31: Results from temperature tests performed at 8 and 10  $\mu\text{l}/\text{min}$ .

### 6.3.4 Main Results

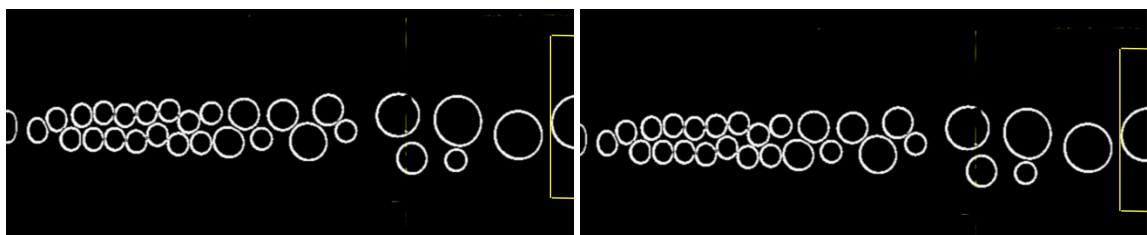
The dispersed flow rate tests at 8 and 10  $\mu\text{l}/\text{min}$  contribute to the main results from the microfluidic experiments. The former dispersed and continuous flow rate tests were performed with demulsifier concentrations at 5 and 25 ppm. Considering the bottle test measurements which were performed with similar chemical demulsifiers, the water cut was significantly much higher for these tests [97]. Therefore, the concentrations were decreased to 0.5 and 2.5 ppm to obtain a similar surface coverage by the demulsifier for the microfluidic experiments as for the bottle test measurements [97].

At high dispersed flow rates at 8 and 10  $\mu\text{l}/\text{min}$ , the coalescence behaviour was studied by counting droplets of specific size classes. As coalescence was present early at the main channel at such high water volumes, recordings were done only at the inlet of the main channel. Compared to the dispersed flow rates at 3 and 4  $\mu\text{l}/\text{min}$  which were recorded both at inlet and outlet as the tendency of coalescence were rather small at the inlet. Therefore, the procedure for detection and quantification of coalescence changed by increasing the dispersed flow rate. Figure 32 and 33 shows a comparison of the different procedures in the software ImageJ to detect quantification at the different flow rates at 3 and 4  $\mu\text{l}/\text{min}$ , and 8 and 10  $\mu\text{l}/\text{min}$ , respectively.



(a) Inlet window. Width  $\sim 50\mu\text{m}$ . (b) Outlet window. Width  $\sim$  largest droplet.

Figure 32: Droplet count for detection of coalescence for dispersed flow rates at 3 and 4  $\mu\text{l}/\text{min}$ .



(a) Inlet window. Width  $\sim 50\mu\text{m}$ . (b) Inlet window. Width  $\sim 70\mu\text{m}$ .

Figure 33: Droplet count for detection of coalescence for dispersed flow rates at 8 and 10  $\mu\text{l}/\text{min}$ .



The recordings included 11 147 frames at 2000 frames/s for approximately 7 seconds for the 8 and 10  $\mu\text{l}/\text{min}$  dispersed flow rates. The study involved analysis of initially generated droplets (size 1) and two coalesced initial size droplets (size 2). The size classes included a close to constant range of area at a constant flow rate. The size 1 droplets involved areas between 800-1500  $\mu\text{m}^2$ , and the size 2 droplets ranged between 2500 - 3100  $\mu\text{m}^2$  which were specified in the Analysis Particles function in ImageJ. To obtain reliable data input, the detection window was decreased to a minimum for counting the droplets in both size classes. As the maximum droplet diameter for size class 1 and 2 was approximately 50 and 70  $\mu\text{m}$ , respectively, the width was adjusted to these values to eliminate duplicate count of objects.

By comparing the total volume of each size class with the total volume of water flow in, it was possible to obtain information about the tendency of coalescence. Considering the uniform depth of the coalescence chamber, some droplets in size class 2 underwent squeezing due to a large diameter, which is visualized in Figure 34. The volume calculation is shown in Appendix B.

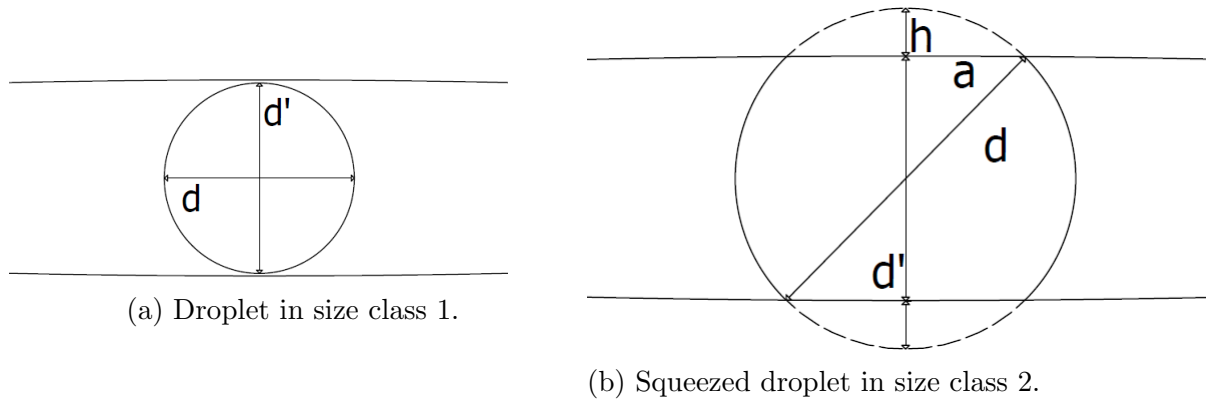


Figure 34: Droplets in size class 1 and 2.

Based on the volume calculation, the percentage of total water droplet volumes of each size class were found. The results are shown in Figure 35 for the dispersed flow rate at  $8 \mu\text{l}/\text{min}$ .

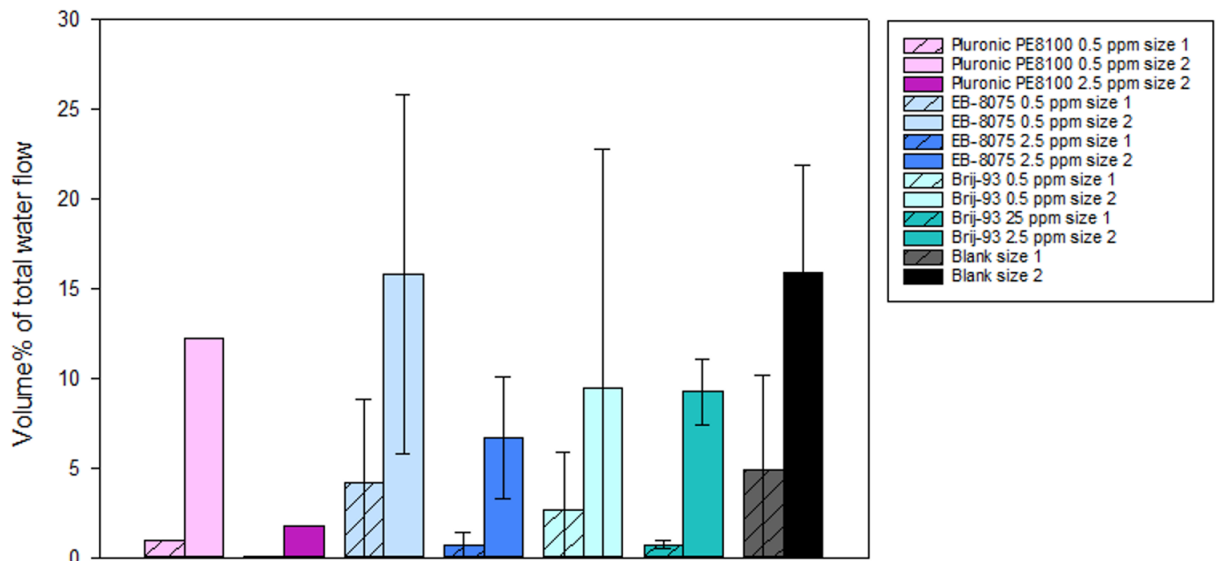


Figure 35: Volume% of size class 1 and 2 droplets at dispersed flow at  $8 \mu\text{l}/\text{min}$ .

The tests with dispersed flow rates at  $8 \mu\text{l}/\text{min}$  indicate overall a relatively high volume% of water droplets in size class 1 and 2. Pluronic PE8100 does not include standard deviations due to certain problems related to minimization of the initial generated droplets during testing of the two other parallels. The error was probably caused due to fibres stuck in the meandering channels which disturbed the continuous water flow of water. One of the main findings when unexpected problems occurred, was that even small particles could split the water flow and disturb the overall tendency of coalescence. Such tests were not valid and frequently discarded. It is also worth mentioning that the image analysis probably provided sources of error as the editing of contrast and brightness had an impact on the size of droplet film. Poor editing may have caused the droplet area to be miscalculated from the image analysis.

Considering the different crude oil systems with demulsifier concentrations at 0.5 and 2.5 ppm, a significant trend is the decrease of water droplets at size class 1 and 2 when the demulsifier concentrations were increased. The results indicate that the tendency of collisions between the initial generated droplets is high, and higher size classes are present in the inlet of the coalescence chamber. According to the bottle tests performed in earlier experiments [97], the Pluronic PE8100 and EB-8075 at high concentrations have proven to be most efficient. The behaviour is reflected in the microfluidic experiments. Overall, the original crude oil system without chemical

additives provides information about the highest fraction of small droplets compared to the systems with demulsifier.

The volume% of total water flow of size class 1 and 2 at dispersed flow rates at  $10 \mu\text{l}/\text{min}$  is shown in Figure 36.

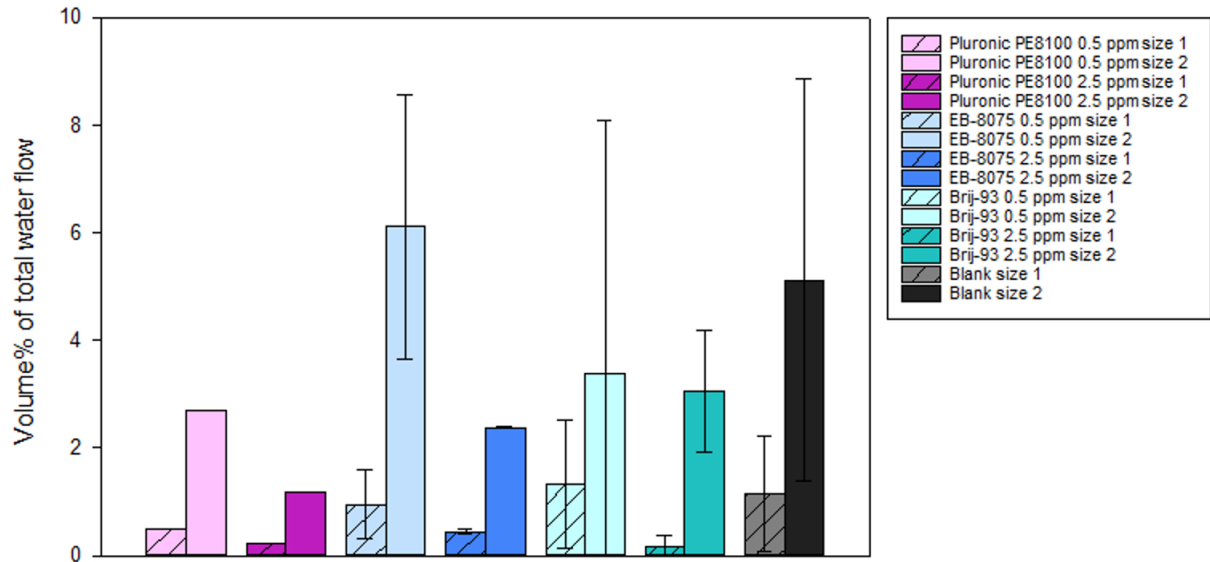


Figure 36: Volume% of size class 1 and 2 droplets at dispersed flow at  $10 \mu\text{l}/\text{min}$ .

The results show a great tendency of coalescence for Pluronic PE8100 at 2.5 ppm with a volume% of total water flow at approximately 1.5 % for size 2. Number of droplets for both size classes are significantly high, which indicate that higher size classes are present at the inlet of the channel. The tendency of coalescence is rather different for EB-8075 at 0.5 ppm. The values reflect high numbers of size class 2, which indicate that low coalescence is present. While Brij-93 provide almost equal fractions of droplets of size 2 for both concentrations, the amount of size 1 is relatively lower for the higher concentration.

According to the optimum oil/water ratios for phase separation, systems with high amounts of water become less stable compared to systems with a low water fraction. High number of dispersed water droplets indicate a high probability for efficient collisions. The tendency of collisions are greatly expressed in the dispersed water flow rate tests at 8 and  $10 \mu\text{l}/\text{min}$  as the fraction of size class 1 and 2 is significantly lower at higher water flow rates.

The complementary IFT and QCM-D measurements provided valuable information for verification of the microfluidic experiments. As the ability to provide separation depends on several factors, the IFT measurements gave necessary indications on the reduction of interfacial tensions for all systems. By comparing the main re-

sults from the microfluidic measurements with the IFT results, one see a clear trend from both tests. Pluronic PE8100 at 25 ppm gives the lowest amount of droplets in size class 1 and 2 for flow rates at 8 and 10  $\mu\text{l}/\text{min}$ , which may be verified by the IFT results which show that the system provides the largest reduction in IFT. The results indicate that the system includes high tendency of coalescence as the smallest droplet sizes are not present in the inlet of the coalescence chamber. It indicates that high coalescence frequently occur early at the chamber, compared to the other systems. Which may be due to fast adsorption of demulsifier which improve the tendency of coalescence by among other things reducing the interfacial tension between the two phases. The results do also indicate that the EB-8075 at 25 ppm has a relatively similar trend for both tendency of coalescence and reduction in IFT which verify the performance of demulsifier in droplet coalescence detected in the microfluidic experiments.

But as an assessment of the efficiency of a demulsifier does not depend only on the ability to reduce interfacial tension, the QCM-D measurements were a suitable complementary performance for verification to obtain valuable information about the physical properties during adsorption of the surface-active additives to a hydrophilic surface, in addition to reaction kinetics, through a relative change in frequency and dissipation. It is worth mentioning that some of the results indicated no conformation to the microfluidic tests, but some significant trends are worth highlighting. From the behaviour of dissipation of the Pluronic PE8100, one assess a rapid adsorption which may be reflected in the fast and large reduction in IFT, in addition to the high tendency of coalescence in the microfluidic experiments.

## 6.4 Complementary Bottle Test Results

The results from the bottle tests performed in an earlier study are presented in Figure 37, 38 and 39 [97].

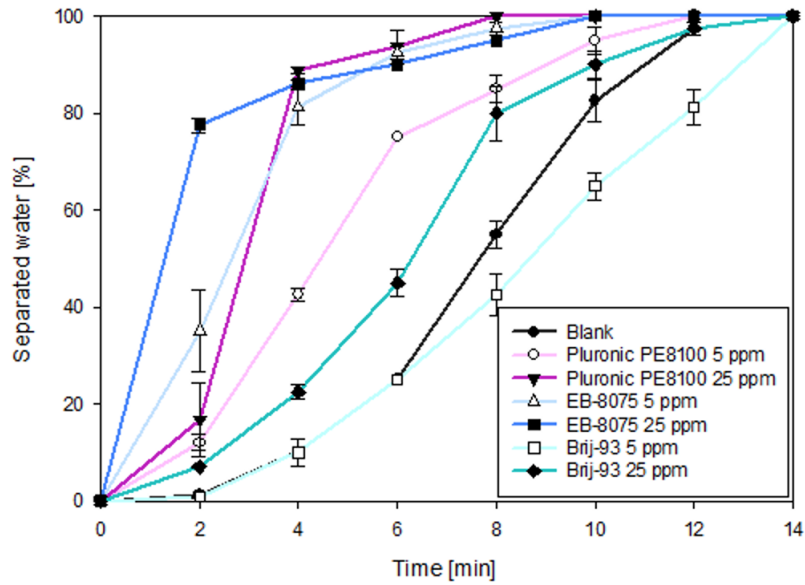


Figure 37: Separated volume at 40% water cut.

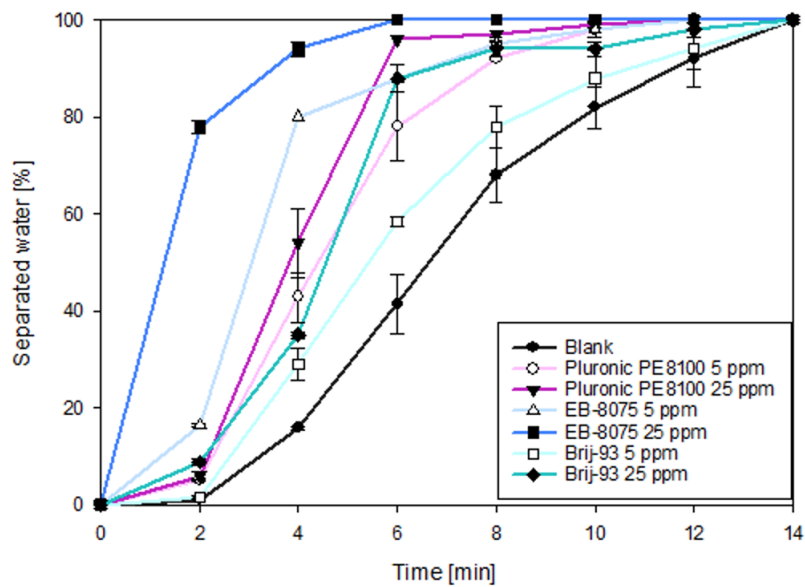


Figure 38: Separated volume at 50% water cut.

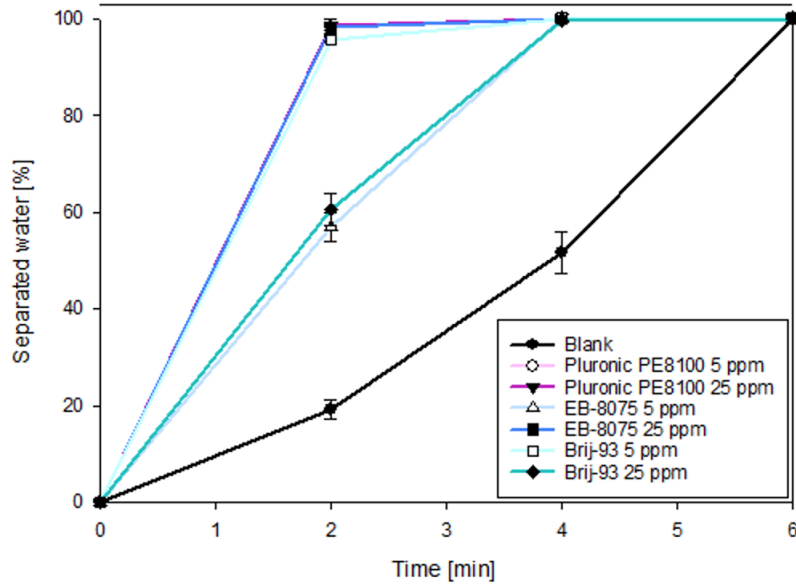


Figure 39: Separated volume at 60% water cut.

The bottle tests were performed by varying several parameters such as temperature, water cut and chemical demulsifier concentration. The performance of microfluidics was done in a similar way. The temperature was adjusted by the use of a steel syringe with adjustable set temperature. The water/oil ratio was regulated by varying the dispersed and continuous flow rate, and the demulsifier solutions were prepared in oil samples with different concentrations. These three parameters which concern the kinetics of the system have proven to be useful to study and assess the separation of a crude oil emulsion. It is possible to draw several similarities from the microfluidic experiments and the bottle tests. The main factors might be the increase in chemical demulsifier which affect all the systems in an equal way, by improving destabilization through phase separation and tendency of coalescence. The variation of oil/water ratio does also affect the efficiency of demulsification in both methods. The destabilization process got accelerated by increasing the water cut or dispersed water flow rate.

By comparing the separation efficiency in the bottle test results for the three demulsifiers with the original system without addition of destabilizing chemicals, one can see that the Brij-93 demulsifier provided the less efficient separation. The rate of separation is even lower than the original system for some systems with demulsifier which is also reflected in the microfluidic experiments through a low tendency of coalescence.

The ability to improve phase separation and tendency of coalescence for the three demulsifiers is attributed not only to the high variations in surface activity, but also the differences related to the chemical structures and the molecular weight which is indicated in the results from both the microfluidic experiments and the bottle tests. By studying the separated water phase as a function of time in the bottle test results, one can notice that all of the demulsifier systems show a quite fast initial separation. According to the theory about the chemical model demulsifier structures, one can notice that the high molecular weight block copolymer Pluronic PE8100 promoted a more effective separation compared to Brij-93 with a lower molecular weight. Considering the tendency of coalescence in the microfluidic experiments, the polymeric Pluronic demulsifier showed a much higher ability to improve coalescence compared to the other two demulsifiers. The high surface-activity and fast ability of adsorption of Pluronic PE8100 were also reflected in both the IFT and QCM-D measurements.

As mentioned, the kinetic parameters are useful to study to assess the separation efficiency of crude oil emulsions. Conventional separation methods such as bottle tests may not be suited for stability analysis, as the systems do not include the external flow field which will have a significant impact on the dispersed droplets. However, microfluidic experiments have the possibility to take this factor into account. The latter method does neither include physical emulsion preparation such as the bottle test. As the procedure included manual shaking, it will automatically decrease the reproducibility of such tests. The microfluidic methods does include almost 10 times lower sample volume of oil compared to the bottle tests, which provide the method health and safety benefits.

## 7 Conclusion

As a main conclusion from the microfluidic experiments, the optimized method seemed to provide reliable results as the significant trend conformed the results from the IFT, QCM-D and bottle test measurements. According to the assessment of the most efficient demulsifier, Pluronic PE8100 and EB-8075 at high concentrations have proven to be efficient surface-active chemical additives for the studied systems. The components have shown fast and effective phase separation in the bottle testing, fast and high surface activity to reduce the interfacial tension between the systems and high ability to adsorb on hydrophilic surfaces in the QCM-D measurements. Overall, the efficiency is probably dependent on several physical properties such as molecular weight, chemical structure and wetting properties.

Considering the results from the bottle testing, there are significant trends which are important to emphasize. By comparing the conventional method with the quite new developed technology, there are several benefits with using microfluidics to study destabilization phenomena and testing different production chemicals. The method requires much smaller sample volumes compared to the bottle testing, relatively small sample preparation, fast analysis time and it serves a well established procedure to study kinetic parameters. The procedure includes automatic functionalities which enhance the overall procedure with automatic filling, cleaning and adjustment of water and crude oil fractions.

This study included the assessment of coalescence of water droplets in a continuous oil phase which involved the detection of the tendency of coalescence by calculating the coalescence frequency and study droplet size distribution. According to the determination of droplet size distribution, the study could get expanded by studying higher droplet size classes to obtain a more detailed information about the actual coalescence in each system. The procedures express the flexibility of the technology, as determination of destabilization processes may be detected in several manners. Compared to the bottle test procedure which focuses on the elementary phase separation and not include important factors which actually have a significant impact on the destabilization process and the dispersed system, such as the external flow field.

The basic principle behind the microfluidic method is easy to practice, but several problems occurred during performance. Considering that the systems involve dispersed water droplets in a continuous oil phase, unexpected problems took place. Some of them probably originated from the multicomponent continuous phase. The



unpredictable disturbances during performance were eliminated to a minimum to implement modifications to the W/O systems which seemed to enhance the procedure to a certain degree. It is also worth to mention that even though the method is quite suitable for this specific crude oil, the procedure may not fit a crude oil with a different composition. On the other hand, another crude oil might perform an ideal flow behaviour for this flow setup compared to the crude oil included in this assessment. Even though several improvements were implemented to facilitate the procedure for W/O systems, the method expressed high sensitivity as a small airborne particle could discard a test.

Despite fluctuations in performance, the method would probably serve highly reproducible measurements if certain parts of the procedure got further improved. Permanent hydrophobic coating and filtration of heavy components in the crude oil could improve and progress the technology. According to the overall principle and performance, it is a method which has several advantages compared to conventional methods. If certain improvements and further development are implemented, the technology would probably provide several benefits in the petroleum industry.

## References

- [1] Aavos International. Upstream, midstream, downstream (oil industry). "<https://aavos.eu/glossary/upstream-midstream-downstream-oil-industry/>", 2017.
- [2] Ayhan Demirbas and Osman Taylan. Removing of resins from crude oils. *Petroleum Science and Technology*, 34(8):771–777, 2016.
- [3] Sofiah Atirah Raya, Ismail Mohd Saaid, Abdelazim Abbas Ahmed, and Abubakar Abubakar Umar. A critical review of development and demulsification mechanisms of crude oil emulsion in the petroleum industry. *Journal of Petroleum Exploration and Production Technology*, pages 1–18, 2020.
- [4] Yiu-hung Yau, Victor Rudolph, Kin-chung Ho, Cat Chui-man Lo, and Kam-chau Wu. Evaluation of different demulsifiers for marpol oil waste recovery. *Journal of water process engineering*, 17:40–49, 2017.
- [5] R Kirkpatrick and CL Muhlstein. Performance and durability of octadecyltrichlorosilane coated borosilicate glass. *Journal of non-crystalline solids*, 353(27):2624–2637, 2007.
- [6] Josefina Viades-Trejo and Jesús Gracia-Fadrique. Spinning drop method: from young–laplace to vonnegut. *Colloids and Surfaces A: Physicochemical and Engineering Aspects*, 302(1-3):549–552, 2007.
- [7] BiolinScientific. The qcm-d principle. "<https://www.biolinscientific.com/faq/the-qcm-d-principle>", 2020.
- [8] Marcin Dudek, Are Bertheussen, Thomas Dumaire, and Gisle Øye. Microfluidic tools for studying coalescence of crude oil droplets in produced water. *Chemical Engineering Science*, 191:448–458, 2018.
- [9] Sikkerhetsdatablad alvheim blend crude oil, 2015.
- [10] Merck. Brij 93. "<https://www.sigmaaldrich.com/>", 2020.
- [11] BASF Aktiengesellschaft. Pluronic pe types. "<http://www.timing-ouhan.com/pluronicpetypes.pdf>", 1996.
- [12] MN Ilman et al. Analysis of internal corrosion in subsea oil pipeline. *case studies in Engineering Failure Analysis*, 2(1):1–8, 2014.

- [13] Marcin Dudek, Kelly Muijlwijk, Karin Schroën, and Gisle Øye. The effect of dissolved gas on coalescence of oil drops studied with microfluidics. *Journal of colloid and interface science*, 528:166–173, 2018.
- [14] James G Speight. *The chemistry and technology of petroleum*. CRC press, 2014.
- [15] James J Sheng. *Modern chemical enhanced oil recovery: theory and practice*. Gulf Professional Publishing, 2010.
- [16] AJG Barwise. Role of nickel and vanadium in petroleum classification. *Energy & Fuels*, 4(6):647–652, 1990.
- [17] Norwegian Petroleum. How is petroleum formed? <https://www.norskpetroleum.no/en/petroleum-resources/petroleum-formation/>, 2017.
- [18] Tarek Ahmed. Chapter 14-principles of waterflooding. *Ahmed, T. Reservoir Engineering Handbook*, pages 909–1095, 2006.
- [19] Schlumberger. The defining series: Multilateral wells. "<https://www.slb.com/resource-library/oilfield-review/defining-series/defining-multilateral-wells>", year = 2016.
- [20] Tomas Nordeide Hjartnes. *Synergy between chemical demulsification and electrocoalescence: From bench to large scale*. PhD thesis, Norwegian University of Science and Technology, 2020.
- [21] Schlumberger. Primary recovery. [https://www.glossary.oilfield.slb.com/en/Terms/p/primary\\_recovery](https://www.glossary.oilfield.slb.com/en/Terms/p/primary_recovery)", 2020.
- [22] Albert Barrabino. *Phase inversion, stability and destabilization of model and crude oil water-in-oil emulsions*. PhD thesis, Norwegian University of Science and Technology, 2014.
- [23] Schlumberger. Reservoir pressure. "[https://www.glossary.oilfield.slb.com/Terms/r/reservoir\\_pressure.aspx](https://www.glossary.oilfield.slb.com/Terms/r/reservoir_pressure.aspx)", 2020.
- [24] Marcin Dudek. *Produced water quality and microfluidic methods for studying drop-drop and drop-bubble interactions in produced water*. PhD thesis, Norwegian University of Science and Technology, 2018.
- [25] Schlumberger. Secondary recovery. "<https://www.glossary.oilfield.slb.com/s>", 2020.

- [26] Abdul Rahman El-Nassir. *The effect of interfacial tension on waterflood oil recovery*. PhD thesis, University of Southern California, 1972.
- [27] Magali Christensen and Yukie Tanino. Waterflood oil recovery from mixed-wet limestone: dependence upon the contact angle. *Energy & Fuels*, 31(2):1529–1535, 2017.
- [28] Schlumberger. Enhanced oil recovery. [https://www.glossary.oilfield.slb.com/Terms/e/enhanced\\_oil\\_recovery.aspx](https://www.glossary.oilfield.slb.com/Terms/e/enhanced_oil_recovery.aspx), 2020.
- [29] Chang Samuel Hsu and Paul R Robinson. *Springer handbook of petroleum technology*. Springer, 2017.
- [30] Jacob A Moulijn, Michiel Makkee, and Annelies E Van Diepen. *Chemical process technology*. John Wiley & Sons, 2013.
- [31] U.S. Energy Information Administration. Oil and petroleum products explained - use of oil. "<https://www.eia.gov/energyexplained/oil-and-petroleum-products/use-of-oil.php>", 2019.
- [32] Jiangbo Wen, Jinjun Zhang, Zhihui Wang, and Yongxing Zhang. Correlations between emulsification behaviors of crude oil-water systems and crude oil compositions. *Journal of Petroleum Science and Engineering*, 146:1–9, 2016.
- [33] Siavash Ashoori, Mehdi Sharifi, Mohammad Masoumi, and Mehdi Mohammad Salehi. The relationship between sara fractions and crude oil stability. *Egyptian Journal of Petroleum*, 26(1):209–213, 2017.
- [34] Peiqi Qiao, David Harbottle, Plamen Tchoukov, Jacob Masliyah, Johan Sjoblom, Qingxia Liu, and Zhenghe Xu. Fractionation of asphaltenes in understanding their role in petroleum emulsion stability and fouling. *Energy & Fuels*, 31(4):3330–3337, 2017.
- [35] Keith L Gawrys, P Matthew Spiecker, and Peter K Kilpatrick. The role of asphaltene solubility and chemical composition on asphaltene aggregation. *Petroleum science and technology*, 21(3-4):461–489, 2003.
- [36] Amy M McKenna, Alan G Marshall, and Ryan P Rodgers. Heavy petroleum composition. 4. asphaltene compositional space. *Energy & fuels*, 27(3):1257–1267, 2013.
- [37] SF Wong, JS Lim, and SS Dol. Crude oil emulsion: A review on formation, classification and stability of water-in-oil emulsions. *Journal of Petroleum Science and Engineering*, 135:498–504, 2015.

- [38] Márcia Cristina K de Oliveira, Rogério M Carvalho, Alexandre B Carvalho, Bruno C Couto, Fátima RD Faria, and Rosana LP Cardoso. Waxy crude oil emulsion gel: Impact on flow assurance. *Energy & Fuels*, 24(4):2287–2293, 2010.
- [39] D Langevin, S Poteau, I Hénaut, and JF Argillier. Crude oil emulsion properties and their application to heavy oil transportation. *Oil & gas science and technology*, 59(5):511–521, 2004.
- [40] Tharwat F Tadros. Emulsion formation, stability, and rheology. *Emulsion formation and stability*, 1:1–75, 2013.
- [41] Souleyman A Issaka, Abdurahman H Nour, and Rosli Mohd Yunus. Review on the fundamental aspects of petroleum oil emulsions and techniques of demulsification. *Journal of Petroleum & Environmental Biotechnology*, 6(2):1, 2015.
- [42] S Sharma, P Shukla, A Misra, and PR Mishra. Chapter 8—interfacial and colloidal properties of emulsified systems: Pharmaceutical and biological perspective a2—ohshima, hiroyuki. colloid and interface science in pharmaceutical research and development. makino k. *Colloid and Interface Science in Pharmaceutical Research and Development*, pages 149–172, 2014.
- [43] Gustavo Kume, Manlio Gallotti, and George Nunes. Review on anionic/cationic surfactant mixtures. *Journal of Surfactants and Detergents*, 11(1):1–11, 2008.
- [44] James J Sheng. Chapter 7-surfactant flooding. *Modern chemical enhanced oil recovery*, pages 239–335, 2011.
- [45] LN Mukerjee and SN Srivastava. Finely divided solids as emulsifiers. *Kolloid-Zeitschrift*, 149(1):35–38, 1956.
- [46] Andras Koris, Emma Piacentini, Gyula Vatai, Erika Bekassy-Molnar, Enrico Drioli, and Lidietta Giorno. Investigation on the effects of a mechanical shear-stress modification method during cross-flow membrane emulsification. *Journal of Membrane Science*, 371(1-2):28–36, 2011.
- [47] Murtada Mohammed Abdulredha, Hussain Siti Aslina, and Chuah Abdullah Luqman. Overview on petroleum emulsions, formation, influence and demulsification treatment techniques. *Arabian Journal of Chemistry*, 13(1):3403–3428, 2020.
- [48] Reza Zolfaghari, Ahmadun Fakhru'l-Razi, Luqman C Abdullah, Said SEH El-nashaie, and Alireza Pendashteh. Demulsification techniques of water-in-oil and oil-in-water emulsions in petroleum industry. *Separation and Purification Technology*, 170:377–407, 2016.

- [49] Aleksandar MM Spasic. *Rheology of Emulsions: Electrohydrodynamics Principles*. Academic Press, 2018.
- [50] Margaret M Robins. Emulsions—creaming phenomena. *Current opinion in colloid & interface science*, 5(5-6):265–272, 2000.
- [51] Yunhong Cao, Eric Dickinson, and David J Wedlock. Creaming and flocculation in emulsions containing polysaccharide. *Food Hydrocolloids*, 4(3):185–195, 1990.
- [52] Mooyoung Han and Desmond F Lawler. The (relative) insignificance of  $g$  in flocculation. *Journal-American Water Works Association*, 84(10):79–91, 1992.
- [53] Djamel Ghernaout, Abdulaziz Ibraheem Al-Ghonamy, Ahmed Boucherit, Badiia Ghernaout, Mohamed Wahib Naceur, N Ait Messaoudene, Mohamed Aichouni, Ammar Abdallah Mahjoubi, and Nouredine Ali Elboughdiri. Brownian motion and coagulation process. *American Journal of Environmental Protection*, 4(5-1):1–15, 2015.
- [54] B Xu, W Kang, X Wang, and L Meng. Influence of water content and temperature on stability of w/o crude oil emulsion. *Petroleum science and technology*, 31(10):1099–1108, 2013.
- [55] Nicolas Bremond and Jérôme Bibette. Exploring emulsion science with microfluidics. *Soft Matter*, 8(41):10549–10559, 2012.
- [56] Sun Dezhi, Jong Shik Chung, Duan Xiaodong, and Zhou Ding. Demulsification of water-in-oil emulsion by wetting coalescence materials in stirred-and packed-columns. *Colloids and Surfaces A: Physicochemical and Engineering Aspects*, 150(1-3):69–75, 1999.
- [57] Yong Bai and Qiang Bai. *Subsea engineering handbook*. Gulf Professional Publishing, 2018.
- [58] SINTEF. Electrocoalescence - for water separation from heavy crude oils. "<https://www.sintef.no/globalassets/upload/energi/nyhetsbrev/2012/>", 2012.
- [59] M Balsamo, A Erto, and A Lancia. Chemical demulsification of model water-in-oil emulsions with low water content by means of ionic liquids. *Brazilian Journal of Chemical Engineering*, 34(1):273–282, 2017.
- [60] Kristin Conrad Powell and Anuj Chauhan. Interfacial tension and surface elasticity of carbon black (cb) covered oil–water interface. *Langmuir*, 30(41):12287–12296, 2014.

- [61] Delphine Daniel-David, Isabelle Pezron, Christine Dalmazzone, Christine Noïk, Danièle Clausse, and Ljepša Komunjer. Elastic properties of crude oil/water interface in presence of polymeric emulsion breakers. *Colloids and Surfaces A: Physicochemical and Engineering Aspects*, 270:257–262, 2005.
- [62] Ivan B Ivanov, Krassimir D Danov, and Peter A Kralchevsky. Flocculation and coalescence of micron-size emulsion droplets. *Colloids and Surfaces A: Physicochemical and Engineering Aspects*, 152(1-2):161–182, 1999.
- [63] Yan Zheng, Minying Zheng, Zonghui Ma, Benrong Xin, Ruihua Guo, and Xuebing Xu. Sugar fatty acid esters. In *Polar lipids*, pages 215–243. Elsevier, 2015.
- [64] Eli Ruckenstein. Microemulsions, macroemulsions, and the bancroft rule. *Langmuir*, 12(26):6351–6353, 1996.
- [65] Wanli Kang, Xia Yin, Hongbin Yang, Yilu Zhao, Zitong Huang, Xiaoyu Hou, Bauyrzhan Sarsenbekuly, Zhou Zhu, Pengxiang Wang, Xiangfeng Zhang, et al. Demulsification performance, behavior and mechanism of different demulsifiers on the light crude oil emulsions. *Colloids and Surfaces A: Physicochemical and Engineering Aspects*, 545:197–204, 2018.
- [66] Milton J Rosen and Joy T Kunjappu. *Surfactants and interfacial phenomena*. John Wiley & Sons, 2012.
- [67] Jiangying Wu, Yuming Xu, Tadeusz Dabros, and Hassan Hamza. Effect of eo and po positions in nonionic surfactants on surfactant properties and demulsification performance. *Colloids and Surfaces A: Physicochemical and Engineering Aspects*, 252(1):79–85, 2005.
- [68] Kristiana-Lisette Gosa and Violeta Uricanu. Emulsions stabilized with peo–ppo–peo block copolymers and silica. *Colloids and surfaces A: Physicochemical and engineering aspects*, 197(1-3):257–269, 2002.
- [69] Wenjuan Chen, Jinming Peng, Yanlei Su, Lili Zheng, Lijun Wang, and Zhongyi Jiang. Separation of oil/water emulsion using pluronic f127 modified polyether-sulfone ultrafiltration membranes. *Separation and Purification Technology*, 66(3):591–597, 2009.
- [70] Robert J Good and Manoj K Chaudhury. Theory of adhesive forces across interfaces. 1. the lifshitz-van der waals component of interaction and adhesion. *Fundamentals of Adhesion*, pages 137–151, 1991.

- [71] Wanli Kang, Guolin Jing, Hongyan Zhang, Mingyuan Li, and Zhaoliang Wu. Influence of demulsifier on interfacial film between oil and water. *Colloids and Surfaces A: Physicochemical and Engineering Aspects*, 272(1-2):27–31, 2006.
- [72] Anil Bhardwaj and Stanley Hartland. Dynamics of emulsification and demulsification of water in crude oil emulsions. *Industrial & engineering chemistry research*, 33(5):1271–1279, 1994.
- [73] T Krebs, CGPH Schroën, and RM Boom. Coalescence kinetics of oil-in-water emulsions studied with microfluidics. *Fuel*, 106:327–334, 2013.
- [74] DJ McClements and JN Coupland. Theory of droplet size distribution measurements in emulsions using ultrasonic spectroscopy. *Colloids and Surfaces A: Physicochemical and Engineering Aspects*, 117(1-2):161–170, 1996.
- [75] Gizele Batalha Freitas, Angela C Duncke, Carla N Barbato, Márcia CK de Oliveira, José C Pinto, and Márcio Nele. Influence of wax chemical structure on w/o emulsion rheology and stability. *Colloids and Surfaces A: Physicochemical and Engineering Aspects*, 558:45–56, 2018.
- [76] M Moradi, V Alvarado, and S Huzurbazar. Effect of salinity on water-in-crude oil emulsion: evaluation through drop-size distribution proxy. *Energy & fuels*, 25(1):260–268, 2011.
- [77] M Abdulkadir. Comparative analysis of the effect of demulsifiers in the treatment of crude oil emulsion. *ARPJ Journal of Engineering and Applied Sciences*, 5(6):67–73, 2010.
- [78] Zlata Grenoble and Siwar Trabelsi. Mechanisms, performance optimization and new developments in demulsification processes for oil and gas applications. *Advances in colloid and interface science*, 260:32–45, 2018.
- [79] R Bernewitz, F Dalitz, K Köhler, HP Schuchmann, and G Guthausen. Characterisation of multiple emulsions by nmr spectroscopy and diffusometry. *Microporous and mesoporous materials*, 178:69–73, 2013.
- [80] R Bernewitz, G Guthausen, and HP Schuchmann. Nmr on emulsions: characterisation of liquid dispersed systems. *Magnetic Resonance in Chemistry*, 49:S93–S104, 2011.
- [81] Gustavo R Borges, Gabriela B Farias, Talita M Braz, Leila M Santos, Monique J Amaral, Montserrat Fortuny, Elton Franceschi, Cláudio Dariva, and Alexandre F Santos. Use of near infrared for evaluation of droplet size distribution



- and water content in water-in-crude oil emulsions in pressurized pipeline. *Fuel*, 147:43–52, 2015.
- [82] George M Whitesides. The origins and the future of microfluidics. *Nature*, 442(7101):368–373, 2006.
- [83] DJE Harvie, MR Davidson, JJ Cooper-White, and Murray Rudman. A parametric study of droplet deformation through a microfluidic contraction: Low viscosity newtonian droplets. *Chemical engineering science*, 61(15):5149–5158, 2006.
- [84] DH Flinn, DA Guzonas, and R-H Yoon. Characterization of silica surfaces hydrophobized by octadecyltrichlorosilane. *Colloids and Surfaces A: Physicochemical and Engineering Aspects*, 87(3):163–176, 1994.
- [85] Mark E McGovern, Krishna MR Kallury, and Michael Thompson. Role of solvent on the silanization of glass with octadecyltrichlorosilane. *Langmuir*, 10(10):3607–3614, 1994.
- [86] CP Tripp and ML Hair. An infrared study of the reaction of octadecyltrichlorosilane with silica. *Langmuir*, 8(4):1120–1126, 1992.
- [87] AM Seifert and JH Wendorff. Spinning drop experiments on interfacial phenomena: Theoretical background and experimental evidence. *Colloid and Polymer Science*, 270(10):962–971, 1992.
- [88] Jean-Louis Salager. Principles of the spinning drop tensiometer. *Laboratorio FIRP, Escuela de Ingeniería Química, Universidad de Los Andes, Mérida-Venezuela*, 2005.
- [89] Krüss-Advancing your surface science. Spinning drop tensiometer-sdt. "<https://www.kruss-scientific.com/products/tensiometers/spinning-drop-tensiometer-sdt/>", 2020.
- [90] DataPhysics Instruments. Svt-spinning drop video tensiometer. "<https://www.dataphysics-instruments.com/products/svt/>", 2020.
- [91] Schlumberger. Spinning-droptensiometer. "[https://www.glossary.oilfield.slb.com/en/Terms/s/spinning-drop\\_tensiometer.aspx](https://www.glossary.oilfield.slb.com/en/Terms/s/spinning-drop_tensiometer.aspx)", 2020.
- [92] Mohamad M Ayad, Nagy L Torad, Islam M Minisy, Raja Izriq, and El-Zeiny M Ebeid. A wide range sensor of a 3d mesoporous silica coated qcm electrodes for the detection of volatile organic compounds. *Journal of Porous Materials*, 26(6):1731–1741, 2019.

- [93] NanoScience Instruments. Quartz crystal microbalance (qcm). "<https://www.dataphysics-instruments.com/products/svt/>", 2020.
- [94] Bryan D Vogt, Eric K Lin, Wen-li Wu, and Christopher C White. Effect of film thickness on the validity of the sauerbrey equation for hydrated polyelectrolyte films. *The Journal of Physical Chemistry B*, 108(34):12685–12690, 2004.
- [95] Qsense E-series. Qsense e4 operator manual. "[https://warwick.ac.uk/fac/cross\\_fac/sciencecity/programmes/](https://warwick.ac.uk/fac/cross_fac/sciencecity/programmes/)", 2009.
- [96] Sculpteo. Transparent 3d printing: What are your options. "<https://www.sculpteo.com/blog/2019/11/27/transparent-3d-printing-what-are-your-options/>", 2019.
- [97] Karoline Øverlie Edøy. Coalescence and the influence of demulsifiers in w/o emulsions studied by bottle testing and turbiscan measurements. 2019.

# Appendix A Chip Design

Figure 40 shows a scheme with dimensions of the top standard plate for the three chip designs. The dimensions are given in mm.

Figure 40: Scheme of top standard plate.

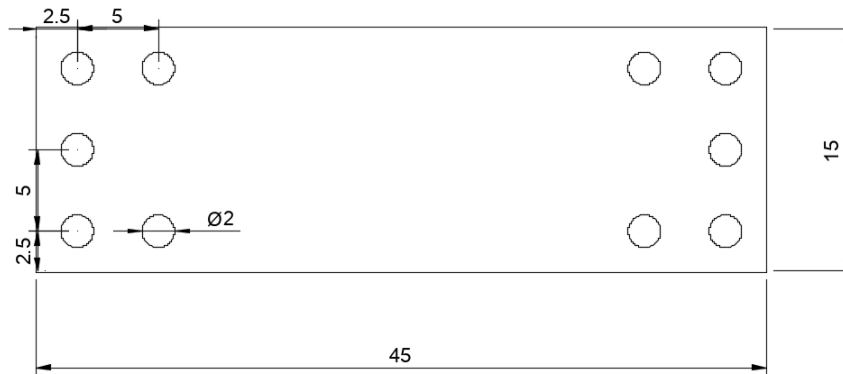


Figure 41 shows a scheme of the bottom plate of chip design 1.

Figure 41: Scheme of bottom plate for chip design 1.

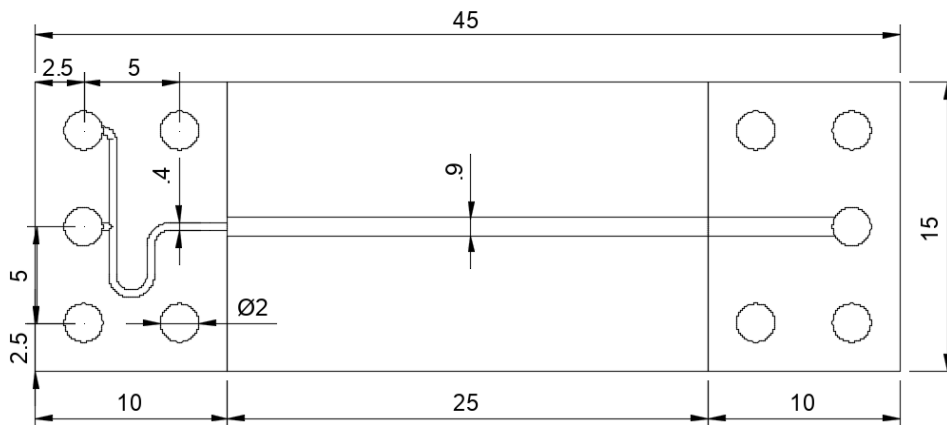
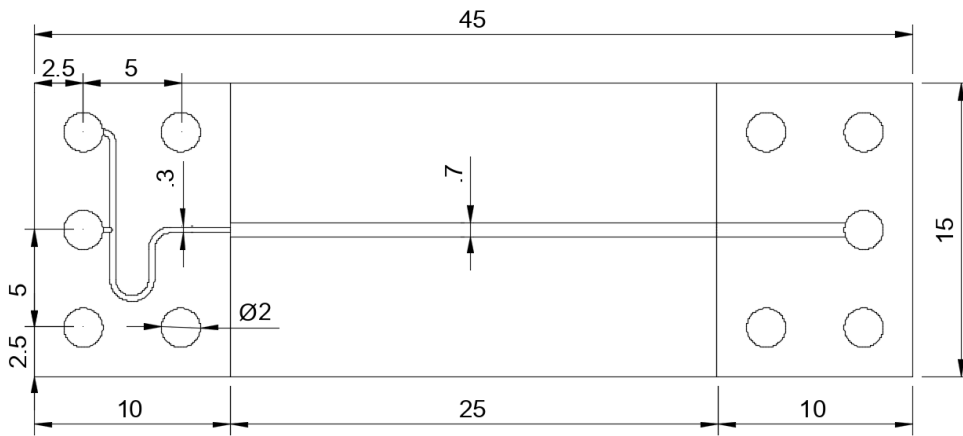


Figure 42 shows a scheme of the bottom plate for chip design 3.

Figure 42: Scheme of bottom plate for chip design 3.



## Appendix B Calculation

Figure 34 shows the schemes of droplets in size class 1 and 2. The volume calculation is based on these schemes.

Calculation of spherical droplet volume is shown in Equation 13.

$$V_{sphere} = \frac{4\pi}{3} \left(\frac{d}{2}\right)^3 \quad (13)$$

$$d = d' \quad (14)$$

$$d \neq d' \quad (15)$$

Calculation of squeezed parts of droplet is shown in Equation 16.

$$V_{crop} = \frac{\pi h}{6} (3a^2 + h^2) \quad (16)$$

$$h = \frac{d - d'}{2} \quad (17)$$

$$a = \sqrt{dh - h^2} \quad (18)$$

Calculation of squeezed droplet volume is shown in Equation 19.

$$V_{CroppedSphere} = V_{Sphere} - 2V_{Crop} \quad (19)$$

